



Research paper

Rational modification, synthesis and biological evaluation of 3,4-dihydroquinoxalin-2(1H)-one derivatives as potent and selective c-Jun N-terminal kinase 3 (JNK3) inhibitors

Xiaodong Dou¹, Huixia Huang¹, Lan Jiang, Guiwang Zhu, Hongwei Jin, Ning Jiao, Liangren Zhang^{*}, Zhenming Liu^{*}, Lihe Zhang

State Key Laboratory of Natural and Biomimetic Drugs, School of Pharmaceutical Sciences, Peking University, Beijing, 100191, China

ARTICLE INFO

Article history:

Received 20 March 2020

Received in revised form

15 April 2020

Accepted 7 May 2020

Available online xxx

Keywords:

JNK3 inhibitors

3,4-dihydroquinoxalin-2(1H)-one

Rational optimization

DDR1/EGFR (T790M

L858R) selectivity

Molecular modeling

ABSTRACT

The c-Jun N-terminal kinase 3 (JNK3) plays key roles in a wide range of diseases, including neurodegeneration diseases, inflammation diseases, cancers, cardiovascular diseases, and metabolic disorders. Previously, we have identified a lead compound, (Z)-3-(2-(naphthalen-1-yl)-2-oxoethylidene)-3,4-dihydroquinoxalin-2(1H)-one (**J46**), which contains a 3,4-dihydroquinoxalin-2(1H)-one core structure as a key fragment to inhibit JNK3. However, compound **J46** displayed high DDR1 and EGFR (T790M, L858R) inhibition and poor physicochemical properties, especially clogD and water-solubility, in its biological studies. Herein, we optimized compound **J46** by structure-based drug design and exploiting the selectivity and physicochemical properties of various warhead groups to obtain compound **J46–37**, which not only exhibited a potent inhibition against JNK3 but also showed more than 50-fold potency better than DDR1 and EGFR (T790M, L858R). Furthermore, the selectivity and structure-activity relationship of novel synthesized 3,4-dihydroquinoxalin-2(1H)-one derivatives were analyzed by molecular docking and molecular dynamics simulation. Overall, compound **J46–37**, as a highly selective inhibitor of JNK3 with well physicochemical properties, is worth developing as therapies for the treatment of diseases related to JNK3.

© 2020 Elsevier Masson SAS. All rights reserved.

1. Introduction

c-Jun N-terminal kinases (JNKs), as the member of serine/threonine protein kinases, belong to the mitogen-activated protein kinase (MAPK) family [1]. JNKs signaling pathway plays as the key regulator in a wide range of cellular functions, including gene expression, neuronal plasticity, cell growth, cell autophagy, and cell apoptosis [2–7]. There are three isoforms of JNKs, JNK1, JNK2, and JNK3, including ten different splice forms of JNKs, sharing more than 82% overall sequence identity and 95% identity in the adenosine 5'-triphosphate (ATP) binding cleft (Fig. 1) [8,9]. In terms of histological distribution, JNK1 and JNK2 are ubiquitously expressed,

while JNK3 is mainly expressed in the brain and to a lesser extent in the heart and testis [10]. Previous studies have indicated that *jnk1* and *jnk2* genes knockout led to the loss of T-cell function, neural tube closure defects, and even embryo death, suggesting that the loss of *jnk1* and *jnk2* might influence the immune cell function and nervous system development [11–13]. Thus, the pharmacological inhibition of JNK1 and JNK2 might lead to the above risk and toxicity, especially in the treatment of chronic diseases with long-term medication. Among them, JNK3 is a multifunctional kinase and phosphorylate a number of downstream substrates, including c-Jun, ATF2, Elk1, DPC4, p53, and NFAT4 [14–16]. Pirianov and co-workers found that *jnk3* gene knockout could protect mice from hypoxic-ischemic brain injury [17]. Furthermore, Yoon and co-workers reported that JNK3 was abnormal and over phosphorylated in the brain of human Alzheimer's disease (AD) patients [18]. Moreover, the JNK3 signaling pathway is frequently over-activated in various cancers, including liver cancer, lung cancer, colon cancer, and breast cancer, and plays as a key regulator in glycolysis in different types of glycolytic tumors, which meant it has an intricate

^{*} Corresponding author. State Key Laboratory of Natural and Biomimetic Drugs, School of Pharmaceutical Sciences, Peking University, Beijing 100191, China.

^{**} Corresponding author. State Key Laboratory of Natural and Biomimetic Drugs, School of Pharmaceutical Sciences, Peking University, Beijing, 100191, China.

E-mail addresses: liangren@bjmu.edu.cn (L. Zhang), zmliu@bjmu.edu.cn (Z. Liu).

¹ These authors contributed equally to this work.

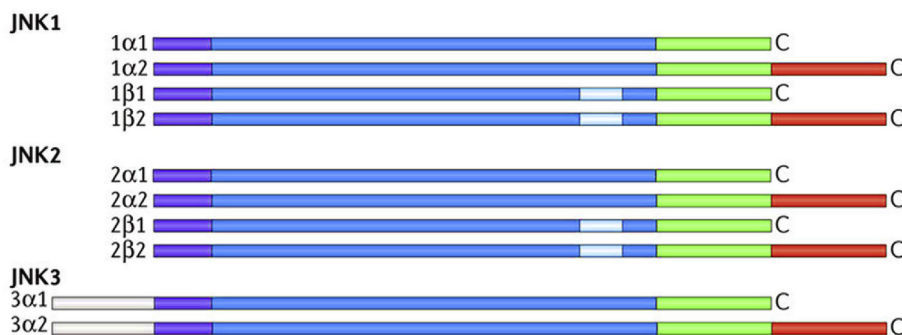


Fig. 1. Schematic representation of the ten different splice forms of JNKs.

relationship with cellular metabolism [19,20]. All of these indicate that JNK3 is involved in the process of many diseases, including neurodegeneration diseases, inflammation diseases, cancers, cardiovascular diseases and metabolic disorders [4,19,21–24]. Therefore, JNK3 is becoming a potential therapeutic target for the development of new drugs.

To date, a series of pan-JNKs inhibitors were reported, but there are no inhibitors on the market (Fig. 2) [1,25,26]. Among them, compound **1** (SP600125) was the first identified pan-JNKs inhibitors, with highly pan-JNKs inhibitory ability, and it was the most commonly used tool molecule in research [27–30]. The clinical trials of two pan-JNKs inhibitors **2** (AS-602801) and **3** (Tanzisertib) are ongoing to treat inflammatory endometriosis and discoid lupus erythematosus, respectively [31–33]. However, the results of the clinical trials were not very promising for the corresponding diseases [34,35]. Thus far, only a few identified isoform-selective JNK3 inhibitors were utilized to understand the mechanism of JNK3 in different diseases. K. Zheng and coworkers reported an aminopyrazole derivative **4**, which displayed highly potent JNK2 and JNK3 inhibition and more than 30-fold selectivity against JNK1 [36]. Furthermore, compound **4** exhibited neuroprotective effect against 6-OHDA induced cell death in vitro. Besides, our group previously reported the indolin-2-one derivative **5** (J30-8) and quinoxaline derivative **6** (J46) with highly potent JNK3 inhibitory

ability and over 2500-fold and 400-fold isoform-selectivity against JNK1/2, respectively [37]. Compound **J30-8** can reverse Alzheimer's disease phenotype in APPswe/PS1dE9 double-transgenic mice by reducing the accumulation of A β and phosphorylated Tau protein.

The aforementioned quinoxaline derivative **6** (J46) was identified by virtual screening from a commercial database [37]. Although compound **J46** displayed a JNK3 IC₅₀ value with 0.25 μ M and significant isoform-selectivity against JNK1 and JNK2, it displayed high DDR1 (IC₅₀ value equal to 0.16 μ M) and EGFR (T790M, L858R) (IC₅₀ value equal to 0.37 μ M) inhibition and poor physicochemical properties, especially clogD and water-solubility. The molecular docking study revealed quinoxaline core as a key fragment to inhibit JNK3 and possible enhancement of selectivity against DDR1 and EGFR (T790M, L858R). Then, structure-based drug design was applied to guide the optimization of lead compound **J46**, and identify a promising candidate for further research. A series of quinoxaline derivatives were synthesized and evaluated, among them, compound **J46-37** exhibited highly potent JNK3 inhibition and more than 500-fold isoform-selectivity against JNK1 and JNK2. Furthermore, compound **J46-37** displayed over 50-fold JNK3/DDR1 and JNK3/EGFR (T790M, L858R) selectivity and improved physicochemical properties compared with the starting compound **J46**. Finally, molecular modeling was performed to

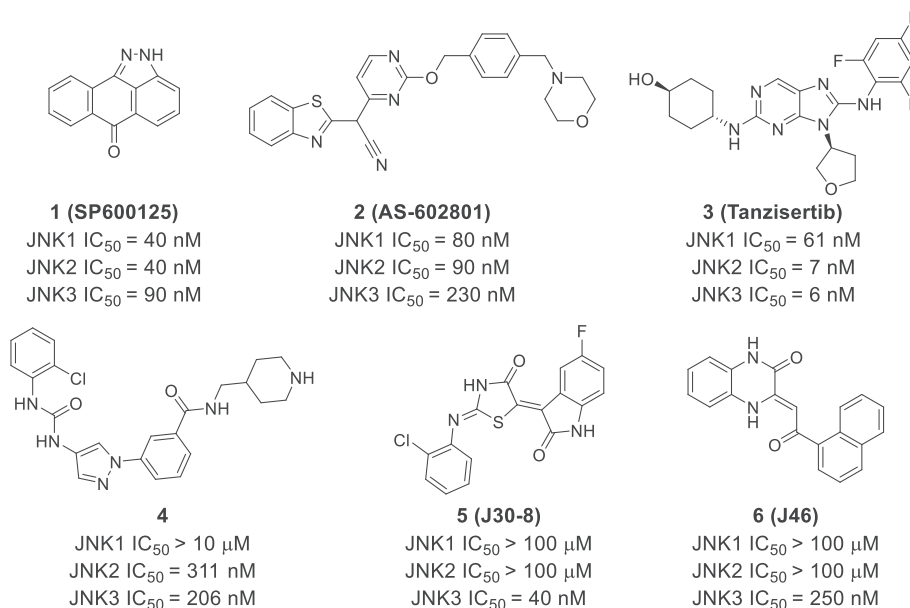


Fig. 2. Chemical structures of representative JNKs inhibitors.

investigate the selectivity and structure-activity relationship (SAR) of quinoxaline analogs.

2. Results and discussion

2.1. Design and synthesis of JNK3 inhibitors

2.1.1. Structure-based design of isoform-selective JNK3 inhibitors

To improve the potency and physicochemical properties of **J46**, two previously identified isoform-selective JNK3 inhibitors, **J30–8** and **J46**, were docked into the ATP-binding cleft of the JNK3 crystal structure (PDB ID: 4W4W) [38]. As shown in Fig. 3, two aforementioned inhibitors exhibited similar binding modes, except that the size of the hydrophobic group inside hydrophobic pocket I (HR I) and the outer hydrophilic substituent. The clogD of **J46** is 3.6, which is not easy to cross the blood-brain barrier (BBB), and the LipE of **J46** is 3.1, which is too low to be a lead compound. To improve the clogD and increase water-solubility of **J46**, the naphthalene ring substituent in **J46** was replaced by substituted benzene ring, for the 2-chlorophenyl group of **J30–8** deeply buried in HR I and showed highly potent JNK3 inhibitory ability and selectivity against JNK1 and JNK2. Furthermore, the outside hydrophilic pocket of ATP-binding cleft in JNK3 could introduce some replacements, especially hydrophilic groups, to improve JNK3 inhibitory activity and increase water-solubility.

To improve selectivity against DDR1 and EGFR (T790M, L858R), compound **J46** was docked into DDR1 (PDB ID: 5BVN) and EGFR (T790M, L858R) (PDB ID: 5HG5), respectively [39,40]. As drawn in Fig. 4A, the binding mode of **J46** in the ATP-binding cleft of DDR1 was very similar to that of **J46** in the ATP-binding site of JNK3. The lactam in the quinoxaline core of **J46** was located at the hinge region of DDR1 and its oxygen atom of carbonyl and hydrogen atom of NH formed two hydrogen bonds to the NH and backbone carbonyl of Met704. The naphthyl group of **J46** was deeply buried in the hydrophobic pocket formed by Val624, Ala653, Lys655, Met676, Ile685, Met699, Ala783 and Phe785. The similarity of the binding modes of **J46** in JNK3 and DDR1 indicates that the selectivity of quinoxaline core JNK3 inhibitor against DDR1 is difficult to achieve. As for EGFR (T790M, L858R), the lactam in the quinoxaline core of **J46** interacted with the EGFR (T790M, L858R) hinge region via two hydrogen bonds with Gln791 and Met793, respectively (Fig. 4B). Interestingly, unlike JNK3 and DDR1, the hydrogen bonds of EGFR (T790M, L858R) were flipped in the hinge region, suggesting that

the selectivity of JNK3 inhibitors, compound **J46**, against EGFR (T790M, L858R) is easy to implement. According to the molecular docking study, the substitution in the benzene ring group would clash with the hydrophobic group inside the hydrophobic pocket of ATP-binding cleft in EGFR (T790M, L858R). The above analysis indicated that the optimization of quinoxaline core should focus on the α -naphthalene ring, to increase inhibitory ability and keep isoform-selectivity, and the 3,4-dihydroquinoxalin-2(1H)-one core, to achieve selectivity to EGFR (T790M, L858R) and improve physicochemical properties, especially water-solubility.

2.1.2. Chemistry

Compounds **J46–16** to **J46–46** were synthesized as illustrated in Scheme 1. We synthesized the building blocks **1a**, **1b**, **1c**, and **1d** from appropriate aminobenzene derivatives (**7** and **8**) through modification of published procedures or known methods [41]. Shortly, the ortho-/meta-substituted aminophenyl acetophenone with Boc anhydride or benzoyl chloride under basic conditions yielded Tert-butyl (2-acetylphenyl)carbamate (**1a**), N-(2-acetylphenyl)benzamide (**1b**), Tert-butyl (3-acetylphenyl)carbamate (**1c**), and N-(3-acetylphenyl)benzamide (**1d**), respectively. The intermediates, substituted heptane-1,3,4-trione, were prepared by naphthalene ethyl ketone or ortho-/meta-substituted acetophenone with oxalic acid diethyl ester using aldol reaction. The intermediates reacted with substituted phenylenediamine to form 3,4-dihydroquinoxalin-2(1H)-one core ring (**J46–16** to **J46–22**, **J46–24** to **J46–31**, and **J46–33** to **J46–46**) [37,42]. The N-Boc deprotection of **J46–25** and **J46–34** was carried out with trifluoroacetic acid (TFA) to give the desired **J46–23** and **J46–32**. The structures of **J46–16** to **J46–46** were characterized by ^1H NMR, ^{13}C NMR, and high-resolution mass spectrometry (HRMS) experiments as single substances.

2.2. JNK3 inhibitory activity and kinases selectivity

2.2.1. JNK3 inhibitory activity and structure-activity relationship

All the novel synthesized compounds were evaluated by JNK3 radiometric assays [37]. Compound **J46** was used as the starting point for the SAR and lead optimization studies and SP600125 was set as the positive control. As shown in Table 1 and Fig. S1, the replacement of the α -naphthyl group of **J46** with a β -naphthyl group (**J46–16**) led to a significant loss of JNK3 inhibition, indicating that the α -naphthalene ring is in a narrow hydrophobic site,

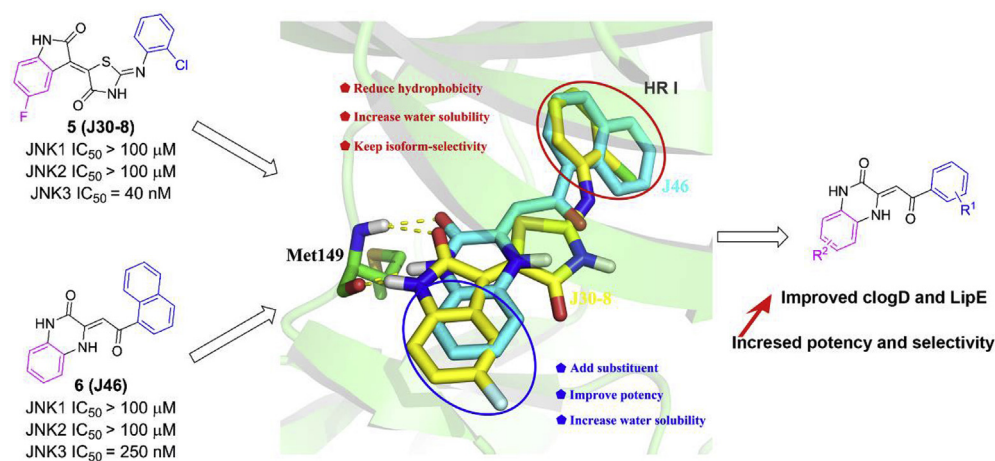


Fig. 3. The design of 3,4-dihydroquinoxalin-2(1H)-one derivatives through structure-based docking design and core hopping. Hydrogen bonds are represented by the yellow lines. The images depict the proposed binding modes generated using PyMOL software. HR I = hydrophobic region I. (For interpretation of the references to colour in this figure legend, the reader is referred to the Web version of this article.)

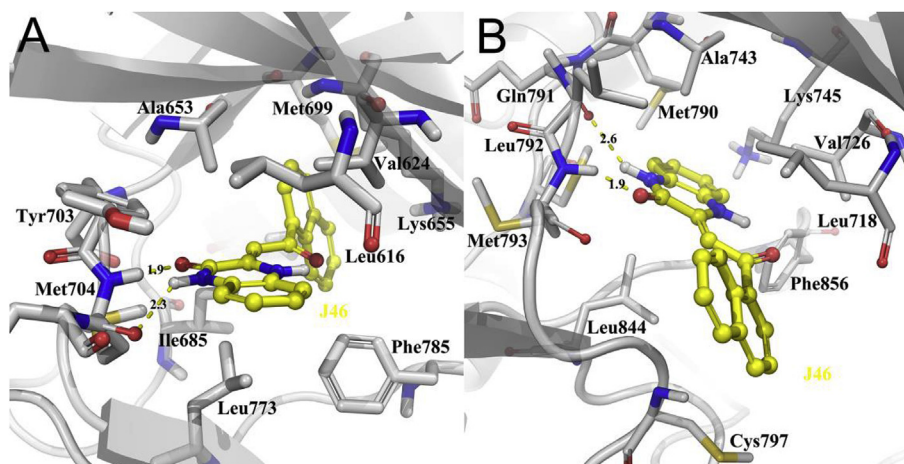
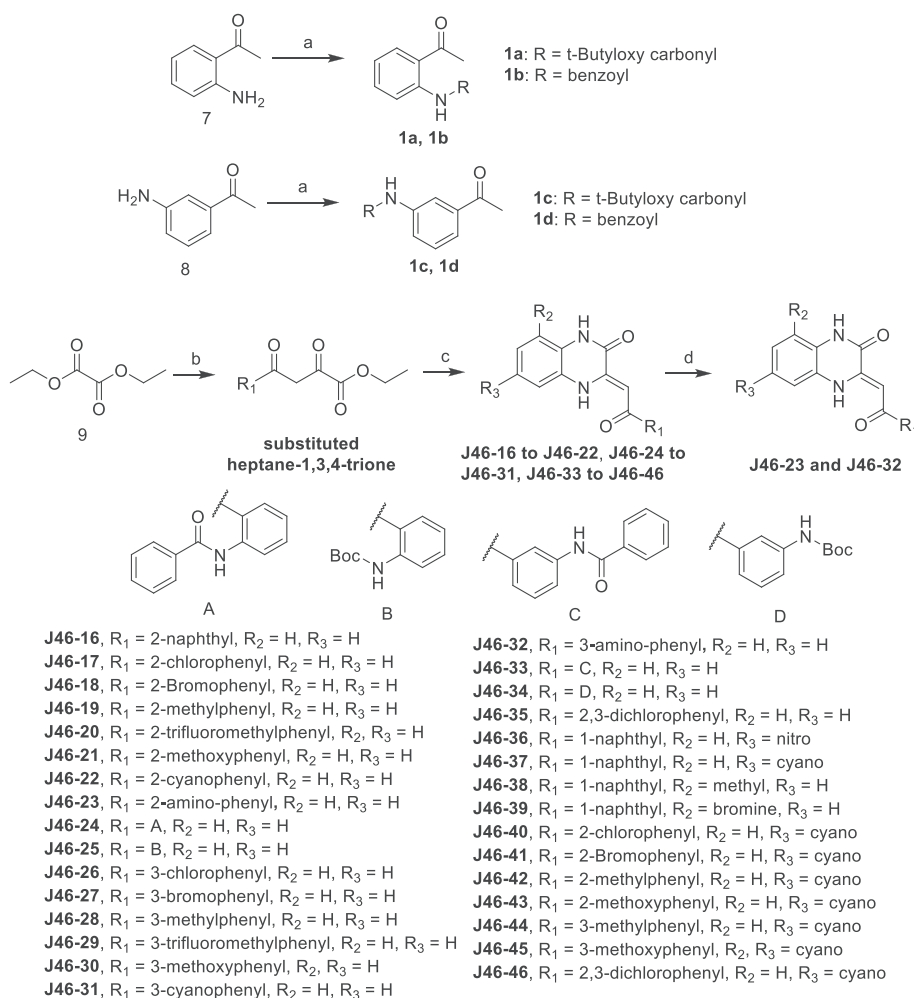


Fig. 4. Predicted binding modes of compound **J46** (yellow) docking with DDR1 crystal protein (PDB code: 5BVN) (A) and EGFR (T790M, L858R) crystal protein (PDB code: 5HG5) (B). Hydrogen bonds are represented by the yellow lines. The images depict the proposed binding modes generated using PyMOL software. (For interpretation of the references to colour in this figure legend, the reader is referred to the Web version of this article.)



^aReagents and conditions: (a) (BOC)₂O, THF, 50 °C, 48h to afford **1a** and **1c**; Benzoyl chloride, Et₃N, DCM, 9h to afford **1b** and **1d**; (b) 2-acetonaphthone or substituted acetophenone, EtONa/EtOH, 0 °C, 30min, then r.t., 4h; (c) substituted O-phenylenediamine, EtOH, r.t., 4h; (d) TFA:DCM = 1:1, r.t., overnight.

Scheme 1. Synthetic Route of the 3,4-dihydroquinoxalin-2(1H)-one derivatives ^a.

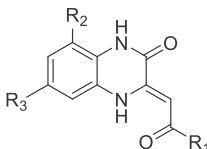
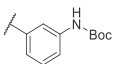
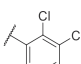
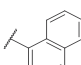
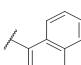
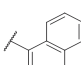
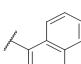
Table 1

Enzymatic activity, chemical structures and representative molecular properties of the synthesized inhibitors of JNK3.

Compounds	R ₁	R ₂	R ₃	Inhibition% (10 μ M)	IC ₅₀ (μ M) ^a	MW ^b	clogD ^c	LipE ^d
SP600125	—	—	—	99 \pm 1	0.09 \pm 0.007	220.2	2.5	4.5
J46		H	H	92 \pm 1	0.25 \pm 0.03	314.3	3.6	3.1
J46-16		H	H	30 \pm 2	ND ^e	314.3	3.6	ND
J46-17		H	H	93 \pm 2	0.41 \pm 0.11	298.7	3.1	3.3
J46-18		H	H	89 \pm 4	1.33 \pm 0.29	343.1	3.2	2.7
J46-19		H	H	82 \pm 2	3.48 \pm 0.32	278.3	3.0	2.5
J46-20		H	H	16 \pm 6	ND	332.2	3.6	ND
J46-21		H	H	84 \pm 2	1.43 \pm 0.26	294.3	2.8	3.0
J46-22		H	H	35 \pm 4	ND	289.2	2.0	ND
J46-23		H	H	66 \pm 2	1.75 \pm 0.34	279.2	2.3	3.5
J46-24		H	H	34 \pm 3	ND	383.4	4.0	ND
J46-25		H	H	17 \pm 4	ND	379.4	3.7	ND
J46-26		H	H	90 \pm 1	0.37 \pm 0.03	298.7	3.1	3.3
J46-27		H	H	13 \pm 2	ND	343.1	3.2	ND
J46-28		H	H	85 \pm 2	0.32 \pm 0.04	278.3	2.9	3.6
J46-29		H	H	21 \pm 4	ND	332.2	3.6	ND
J46-30		H	H	70 \pm 2	5.60 \pm 0.36	294.3	2.7	2.6
J46-31		H	H	2 \pm 2	ND	289.2	1.9	ND
J46-32		H	H	80 \pm 2	0.60 \pm 0.24	279.2	1.7	4.5
J46-33		H	H	11 \pm 4	ND	383.4	3.5	ND

(continued on next page)

Table 1 (continued)

								
J46-34		H	H	64 ± 8	5.15 ± 0.72	379.4	3.4	1.9
J46-35		H	H	91 ± 2	0.43 ± 0.06	333.1	3.5	2.9
J46-36		H	NO ₂	26 ± 3	ND	359.3	2.9	ND
J46-37		H	CN	88 ± 1	0.19 ± 0.03	339.3	2.6	4.1
J46-38		CH ₃	H	16 ± 3	ND	328.3	3.9	ND
J46-39		Br	H	24 ± 3	ND	393.2	4.1	ND

^a Data are presented as geometric mean values of at least two independent runs.

^b Molecular weight.

^c Predicted octanol/water partition coefficient using the *QikProp* module in Schrödinger software.

^d Ligand efficiency, lipE = -logIC₅₀ - clogD.

^e Not determined.

and the β -naphthalene ring replacement would collide with residues deep in the aforesaid pocket, thus the inhibitory activity abolished. Besides, the replacement α -naphthalene ring with the ortho- or meta-substituted benzene ring, the physicochemical properties, clogD, were improved, but the inhibitory ability of JNK3 decreased or disappeared. While small groups including chlorine, methyl, methoxy, and amino groups were introduced into the C-2 or C-3 positions of the benzene ring (J46-17, J46-19, J46-21, J46-23, J46-26, J46-28, J46-30 and J46-32) the activity 1.2–20-fold decreased, and large substituent groups (J46-24, J46-25, J46-33 and J46-34) were introduced, the activities disappeared, indicating that the α -naphthalene ring substitution plays a key hydrophobic role in JNK3 inhibitory ability. While the substituent group is small, the hydrophobic interaction reduced, and the substituent group is too large, the residues in the HR I collided with compounds, thus reducing the inhibitory activity. Furthermore, the replacement of α -naphthalene ring with the ortho- or meta-trifluoromethyl and ortho- or meta-cyano phenyl (J46-20, J46-22, J46-29 and J46-31), the activities were disappeared. These results revealed that the α -naphthalene ring substitution could interact with Lys93 by π -cation interaction, and the strong electron-withdrawing group of the benzene ring will reduce the electron cloud density on the benzene ring, which is not conducive to the formation of π -cation interaction and causes the activity to disappear. Therefore, in a quinoxalinone core structure, the α -naphthalene ring is a suitable substitute for HR I and essential for maintaining JNK3 activity.

The replacement of C-6 in quinoxalinone core with a nitro group (J46-36), led to the JNK3 activity abolished. While cyanyl group (J46-37) was introduced, the JNK3 inhibitory ability increased (IC₅₀ = 0.19 μ M), and the physicochemical properties, clogD (clogD = 2.6) and lipE (lipE = 4.1) were improved, compared with the starting compound J46. The replacement of C-8 in

quinoxalinone core with bromine and methyl groups (J46-38 and J46-39), the activity abolished, which meant that the substitution of C-8 will collide with the residues in the hinge region and cause the significant loss of activity.

To improve the physicochemical properties and keep the isoform-selectivity, compounds J46-40 to J46-46 were designed and synthesized by fixing C-6 of quinoxalinone core with cyano group substitution. As exhibited in Table 2, the SAR is similar to that obtained from compound J46-16 to J46-39. While the α -naphthalene ring in compound J46-37 was replaced by the ortho- or meta-substituted benzene ring, the physicochemical properties, including clogD, were improved, but the inhibitory activity of JNK3 was not increased. Therefore, in the quinoxalinone core compounds, the α -naphthalene ring played a key role in JNK3 inhibitory ability and was suitable to the HR I.

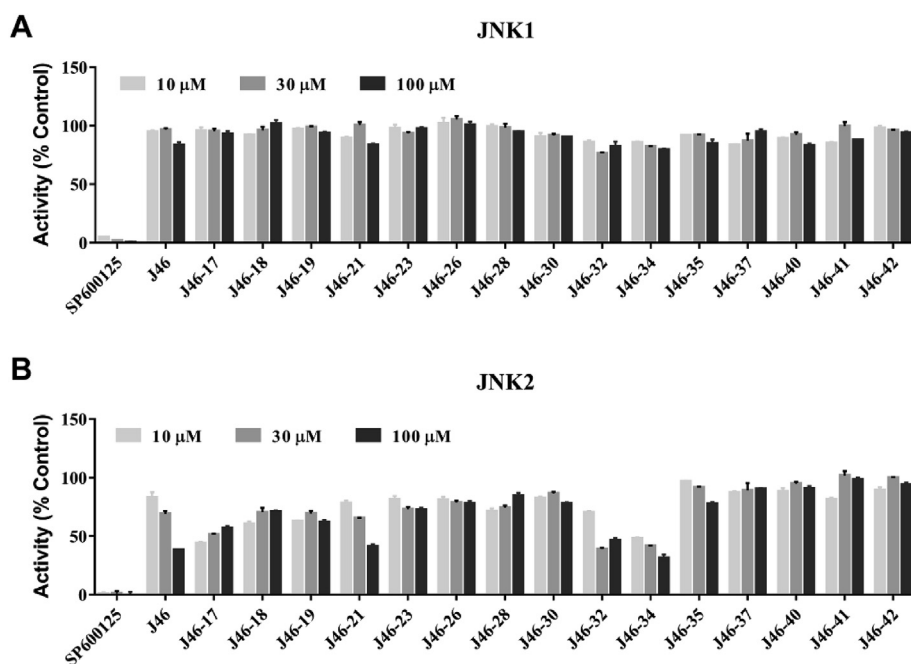
2.2.2. Isoform-selectivity and DDRs/EGFRs selectivity of JNK3 inhibitors

To investigate the isoform-selectivity of the identified JNK3 inhibitors, all of the compounds with JNK3 inhibitory ability were evaluated by JNK1 α 1 and JNK2 α 2 radiometric assays at the concentration of 10, 30, and 100 μ M. As drawn in Fig. 5A and B, the positive compound SP600125, a pan-JNKs inhibitor, exhibited more than 95% inhibition rate against JNK1 α 1, JNK2 α 2, and JNK3 at the concentration of 10, 30, and 100 μ M. Notably, all of the aforementioned JNK3 inhibitors exhibited no inhibition to JNK1 α 1 even at the concentration of 100 μ M, which was consistent with previously reported [37]. As for JNK2 α 2, J46 showed 30% and 60% inhibition to JNK2 α 2 at 30 μ M and 100 μ M, respectively. The replacement of α -naphthalene ring with 2-chlorophenyl, 2-methoxy phenyl, 3-amino-phenyl and N-Boc-3-amino-phenyl groups (J46-17, J46-21, J46-32, and J46-34), were not conducive to JNK2 α 2 selectivity, while the introduction of 2-bromophenyl, 2-

Table 2

Enzymatic activity, chemical structures and representative molecular properties of the synthesized inhibitors of JNK3.

Compounds	R ₁	Inhibition% (10 μ M)	IC ₅₀ (μ M) ^a	MW ^b	clogD ^c	LipE ^d
SP600125	—	99 \pm 1	0.09 \pm 0.007	220.2	2.5	4.5
J46-37		88 \pm 1	0.19 \pm 0.03	339.3	2.6	4.1
J46-40		81 \pm 0	1.68 \pm 0.19	323.7	2.5	3.3
J46-41		63 \pm 2	4.78 \pm 0.64	368.1	2.5	2.8
J46-42		57 \pm 3	7.37 \pm 1.18	303.3	2.3	2.8
J46-43		46 \pm 10	ND ^e	319.3	2.1	ND
J46-44		35 \pm 5	ND	303.3	2.2	ND
J46-45		19 \pm 0	ND	319.3	2.0	ND
J46-46		25 \pm 5	ND	358.1	2.7	ND

^a Data are presented as geometric mean values of at least two independent runs.^b Molecular weight.^c Predicted octanol/water partition coefficient using the *QikProp* module in Schrödinger software.^d Ligand efficiency, lipE = -logIC₅₀ - clogD.^e Not determined.**Fig. 5.** JNK1 (A) and JNK2 (B) inhibitory activity of JNK3 inhibitors at the concentration of 10, 30, and 100 μ M. All of the values are reported as means \pm SE of triplicate.

methylphenyl, 2-amino-phenyl, 3-chlorophenyl, 3-methylphenyl, 3-methoxyphenyl, and 2,3-dichlorophenyl groups (**J46–18**, **J46–19**, **J46–23**, **J46–26**, **J46–28**, **J46–30** and **J46–35**), were conducive to JNK2 α 2 selectivity. Interestingly, the replacement of C-6 of quinoxalinone core with a cyano group (**J46–37**, **J46–40**, **J46–41**, and **J46–42**), the JNK2 α 2 selectivity was always improved, which meant that the cyano group was essential for achieving and maintaining of JNK3 selectivity against JNK2 α 2.

Aim to study selectivity of JNK3 inhibitors against DDR1 and EGFR (T790M, L858R), all of the compounds with JNK3 inhibitory ability were evaluated by DDR1, DDR2, EGFR, EGFR (L858R), EGFR (L861Q), EGFR (T790M), EGFR (T790M, L858R) radiometric assays. As shown in Fig. 6A, all of the replacement of α -naphthalene ring, led to the improvement of selectivity against DDR1, especially 3-chlorophenyl, 3-methoxy phenyl, and N-Boc-3-amino-phenyl groups (**J46–26**, **J46–30**, and **J46–34**) showed no inhibition against DDR1 at 10 μ M. Notably, the replacement of C-6 of quinoxalinone core with the cyano group (**J46–37**, **J46–40**, **J46–41**, and **J46–42**), exhibited excellent selectivity against DDR1. Besides, all of the optimizations did not affect DDR2 activity. As for EGFR (L858R) and EGFR (T790M, L858R) (Fig. 6B), the replacement of α -naphthalene ring with 3-chlorophenyl, 2-methylphenyl, and N-Boc-3-amino-phenyl groups (**J46–26**, **J46–28**, and **J46–34**), led to the significant improvement of selectivity against EGFR (L858R) and EGFR (T790M, L858R). Furthermore, the replacement of C-6 of quinoxalinone core with a cyano group (**J46–37**, **J46–40**, **J46–41**, and **J46–42**), showed no inhibitory ability against EGFR (L858R) and EGFR (T790M, L858R) at 10 μ M, which was consistent with the aforementioned structure-bases drug design. Additionally, all of the optimizations had no significant effect on EGFR, EGFR (L861Q), and EGFR (T790M) activity (Fig. S2). All of these revealed that the replacement of C-6 of quinoxalinone core with cyano group showed no inhibition on DDR1/2 and EGFR, EGFR (L858R)/EGFR (L861Q)/EGFR (T790M)/EGFR (T790M, L858R), which meant the cyano group in C-6 of quinoxalinone core is a key role in achieving JNK3 selectivity against DDRs and EGFRs.

2.3. Binding mode and selectivity analysis of the identified JNK3 inhibitors

As indicated in Fig. 7A, compound **J46–37** exhibited excellent isoform-selectivity against JNK1 α 1 ($IC_{50} > 100 \mu$ M) and JNK2 α 2 ($IC_{50} > 100 \mu$ M), and significant kinases selectivity against DDR1 ($IC_{50} > 10 \mu$ M) and EGFR (T790M, L858R) ($IC_{50} > 10 \mu$ M), compared with **J46** showed DDR1 ($IC_{50} = 0.16 \mu$ M) and EGFR (T790M, L858R) ($IC_{50} = 0.37 \mu$ M) inhibitory ability. To investigate the binding modes and study the structure-activity relationship of 3,4-dihydroquinoxalin-2(1H)-one derivatives, compound **J46–37** was docked into the ATP-binding cleft of JNK3 (PDB ID 4W4W). As drawn in Fig. 7B and C, the binding mode of **J46–37** is similar to that of **J46**. The lactam in the quinoxalin moiety of **J46** was located at the hinge region of JNK3 and its oxygen atom of carbonyl and hydrogen atom of NH form two hydrogen bonds to the NH and backbone carbonyl of Met149. Furthermore, the naphthyl group of **J46–37** is deeply located at the HR I (also called selectivity pocket) [1] and the C-6 cyano group of quinoxalinone core was exposed to the external hydrophilic pocket. To explain the isoform-selectivity of **J46**, the JNK1 (PDB ID: 3PZE) and JNK2 (PDB ID: 3E7O) structures were superimposed to the crystal of JNK3 (PDB ID 4W4W) [43,44]. As shown in Fig. 7D, the α -naphthalene group of **J46–37** is located at the center of HR I and have a collision with the Met108 of JNK1 or JNK2, leading to the loss of inhibitory ability to JNK1 and JNK2. All of the results reveal that the occupation of HR I is essential for maintaining of JNK3 isoform-selectivity against JNK1 and JNK2.

Aim to investigate the JNK3 inhibitor, compound **J46–37**, selectivity to DDR1 and EGFR (T790M, L858R), the **J46–37** was superimposed to the aforementioned binding modes of **J46** with the DDR1 (PDB ID: 5BVN) and EGFR (T790M, L858R) (PDB ID: 5HG5), respectively [39,40]. As drawn in Fig. 8A and B, the binding mode of **J46–37** in the ATP-binding pocket was very similar to that of **J46**, except that the additional cyano group of **J46–37** had a collision with the oxygen atom in the backbone carbonyl of Lue616 from DDR1. Interestingly, it might explain the activity loss of

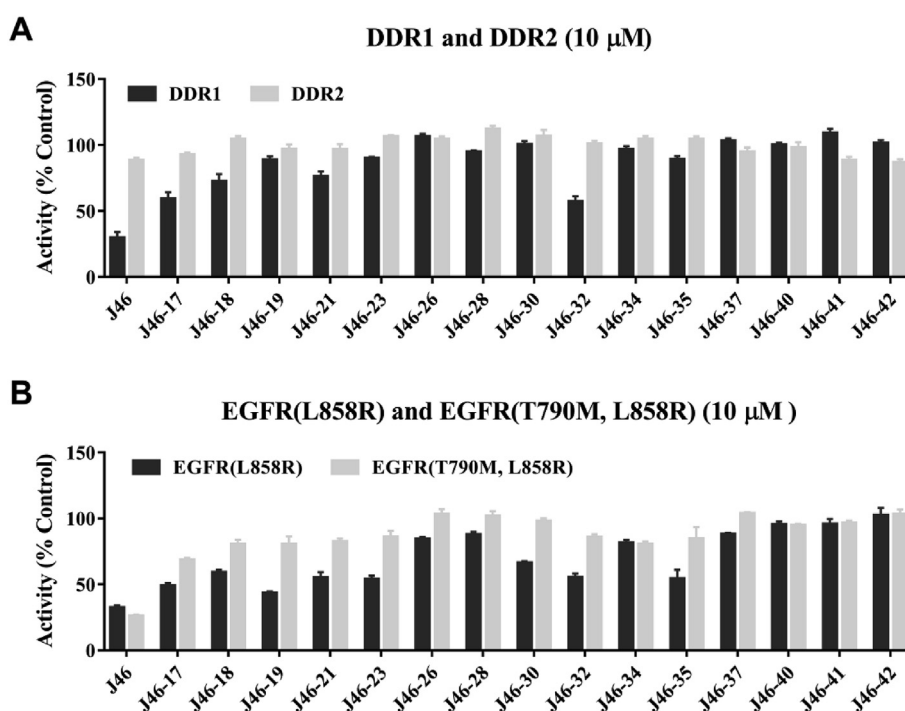


Fig. 6. DDR1/2 (A) and EGFR (L858R)/EGFR (T790M, L858R) (B) inhibitory activity of JNK3 inhibitors at the concentration of 10 μ M. All of the values are reported as means \pm SE of triplicate.

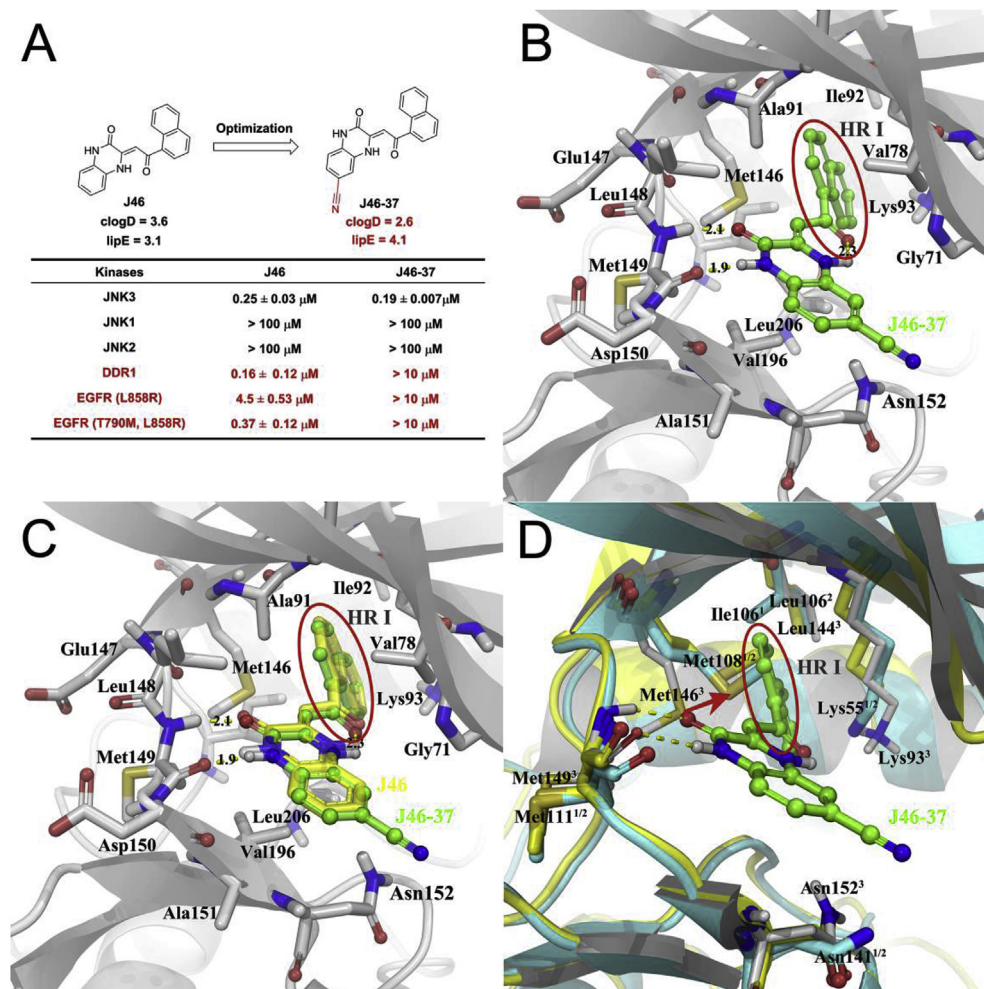


Fig. 7. (A) Structure and physicochemical properties of **J46** and **J46-37**, and IC_{50} values of **J46** and **J46-37** against kinases. IC_{50} values are reported as means \pm SE of duplicate. (B) Predicted binding mode of compound **J46**. (C) Superimposition of the compounds **J46** and **J46-37**. (D) Superimposition of the crystal structures of JNK3 (PDB ID: 4W4W, gray), JNK1 (PDB ID: 3PZE, light blue), and JNK2 (PDB ID: 3E7O, yellow) with compound **J46-37**. Hydrogen bonds are represented by the yellow lines. HR I = hydrophobic region I. Images depicting the proposed binding modes were generated using PyMOL software. (For interpretation of the references to colour in this figure legend, the reader is referred to the Web version of this article.)

J46-37 to DDR1. As for EGFR (T790M, L858R), compound **J46** and **J46-37** exhibited similar binding poses, and the residue Lys745 of EGFR (T790M, L858R) had a collision with the cyano group of **J46-37**, which is consistent with the aforesaid design and biological activity. Thus, the cyano group in the C-6 position of 3,4-dihydroquinoxalin-2(1H)-one core structure is a particular building block to maintain JNK3 selectivity against JNK2, DDR1 and EGFR (T790M, L858R).

To further investigate the binding pattern in the dynamics mode, 50 ns molecular dynamics (MD) simulation was performed for the complex of **J46-37** with JNK3 crystal structure by Desmond software [45]. The complex was stable after 20 ns (Fig. 9A) and the last 30 ns trajectories of MD were extracted and analyzed. As shown in Fig. 9B and C, the results of molecular dynamics are generally consistent with the molecular docking study and the binding mode of **J46-37** did not change. The quinoxalin of **J46-37** formed two hydrogen bonds with the backbone of Met149 over 97% of the simulation time, and the naphthyl group formed π -cation interaction with the side chain of Lys93 during 77% of the simulation time. Furthermore, the oxygen atom of carbonyl linked with naphthalene ring formed an intramolecular hydrogen bond with NH in the quinoxaline core and a water bridge with Lys93 during 77% and 48%

of the simulation time, respectively. Notably, the cyano group in the C-6 position of quinoxaline core formed two water bridges with Ile70 and Ser73, during 14% and 11% of the simulation time, which might explain the moderate improvement of JNK3 inhibitory ability, compared with **J46**. These findings may pave the way to design more optimal JNK3 inhibitors in the future.

3. Conclusion

Previously, compound **J46** was identified as an inhibitor of JNK3 and exhibited potent JNK3 inhibitory ability and selectivity against JNK1 and JNK2. However, compound **J46** showed high DDR1 and EGFR (T790M, L858R) inhibition and poor physicochemical properties in its biological studies. To improve the aforesaid properties in this work, a series of novel 3,4-dihydroquinoxalin-2(1H)-one derivatives were designed and synthesized by SBDD and molecular hybridization. Furthermore, the structure-activity relationship of 3,4-dihydroquinoxalin-2(1H)-one analogs were studied by molecular docking and molecular dynamics simulation. In particular, compound **J46-37**, with a JNK3 IC_{50} value of 0.19 μM, showed 500-fold isoform-selectivity against the JNK1 α 1 and JNK2 α 2 and more than 50-fold selectivity against the DDR1 and EGFR (T790M,

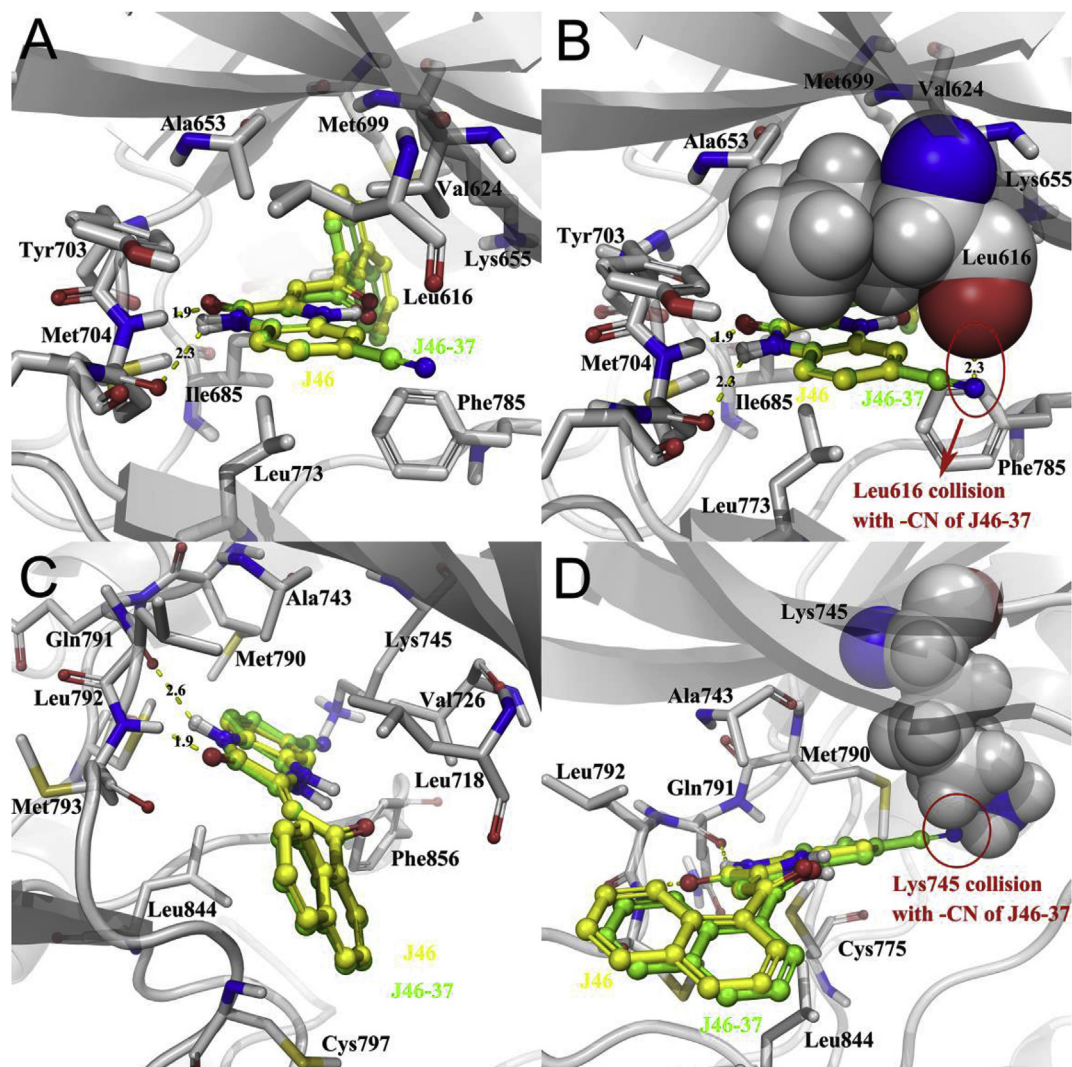


Fig. 8. Front (A) and side view (B) of **J46** (yellow) and **J46-37** (green) with DDR1 (PDB ID: 5BVN). Front (C) and side view (D) of **J46** (yellow) and **J46-37** (green) with EGFR (T790M, L858R) (PDB ID: 5HG5). Hydrogen bonds are represented by yellow lines. Images depicting the proposed binding modes were generated using PyMOL software. (For interpretation of the references to colour in this figure legend, the reader is referred to the Web version of this article.)

L858R). Besides, the physicochemical properties, including clogD and lipE, were improved an order of magnitude, compared with the starting compound **J46**. Overall, compound **J46-37**, as a significantly selective inhibitor of JNK3 with well physicochemical properties, is worth developing as therapies for the treatment of diseases related to JNK3.

4. Experimental section

4.1. Chemistry

General method. Synthesis reagents and solvents were obtained from commercial suppliers and used without further purification. SP600125 was purchased from Selleck Chemicals LLC. Characterizations of compounds are provided in the Supporting Information. Melting points were determined in open capillary tubes on a Büchi melting point apparatus M – 560 and are uncorrected. ^1H and ^{13}C NMR spectra were recorded on Bruker (400 MHz) instruments, using dimethyl sulfoxide ($\text{DMSO}-d_6$) as solvents. Chemical shifts are given in parts per million (ppm) downfield from tetramethylsilane (δ) as the internal standard in deuterated solvent and coupling

constants (J) are in Hertz (Hz). Data are reported as follows: chemical shift, integration, multiplicity (s = singlet, d = doublet, t = triplet, q = quartet, dd = doublet of doublet, ddd = doublet of doublet of doublet, dt = doublet of triplet, m = multiplet, bs = broad signal), and coupling constants. High-resolution mass spectra were recorded on a Bruker Apex IV FTMS mass spectrometer using electrospray ionization (ESI). All compounds tested in biological assays were >95% pure.

4.1.1. *Tert*-butyl (2-acetylphenyl)carbamate (**1a**)

To a mixture of 1-(2-aminophenyl)ethan-1-one (10 mmol, 1.35 g) in THF (15 mL) was added di-*tert*-butyl dicarbonate (40 mmol, 8.72 g) and stirred for 48 h at room temperature. Then, the mixture was concentrated in vacuo and extracted with ethyl acetate and water. The organic layer was separated, washed with brine, dried over MgSO_4 and concentrated in vacuo. The residue was purified by column chromatography (silica gel, eluted with 5–20% ethyl acetate in petroleum ether) to give **1a** (2.2 g, 92%) as a white solid. ^1H NMR (400 MHz, $\text{DMSO}-d_6$) δ 10.83 (s, 1H), 8.24 (d, J = 8.4 Hz, 1H), 8.02 (d, J = 7.9 Hz, 1H), 7.59 (t, J = 7.7 Hz, 1H), 7.13 (t, J = 7.6 Hz, 1H), 2.63 (s, 3H), 1.48 (s, 9H).

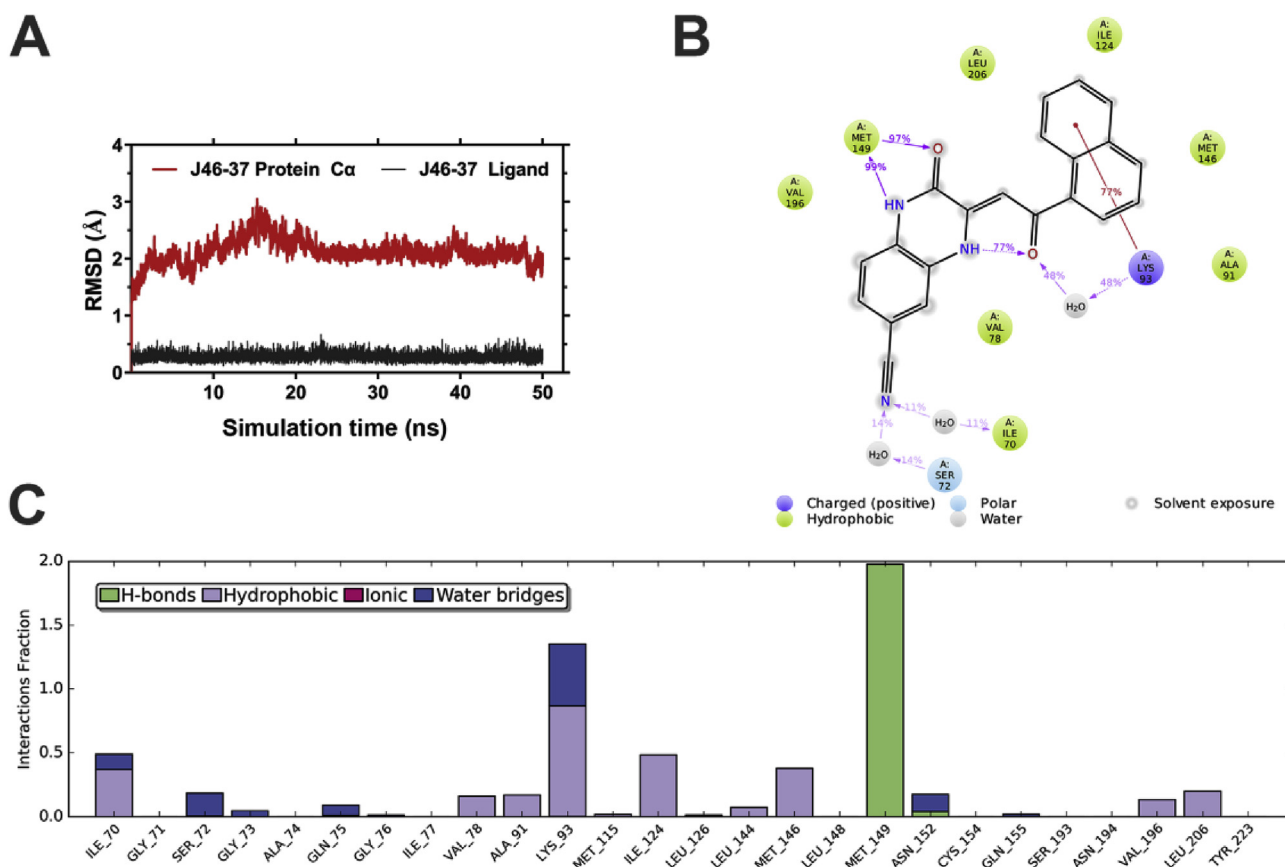


Fig. 9. (A) RMSD of protein and ligand **J46-37** through MD simulations (B) 2D diagram of **J46-37** predicted through MD simulations. Percentage suggests that for X% of the simulation time the specific interaction is maintained. (C) Protein-ligand contacts histogram of **J46-37**.

4.1.2. *N*-(2-acetylphenyl)benzamide (**1b**)

A solution of benzoyl chloride (7.2 mmol, 1.0 g) in THF (10 mL) was dropwise added to the mixture of 1-(2-aminophenyl)ethan-1-one (6 mmol, 0.81 g) and triethylamine (7.2 mmol, 0.72 g) in THF (10 mL) at 0 °C and stirred for another 5 h at room temperature. Then, the mixture was poured into ice water and the pH value was adjusted to 2.0 with hydrochloric acid (2 M). The obtained white solid was filtered and recrystallized from ethanol to give **1b** (1.0 g, 71%) as a white solid. ^1H NMR (400 MHz, $\text{DMSO-}d_6$) δ 12.40 (s, 1H), 8.67 (d, J = 8.4 Hz, 1H), 8.12 (d, J = 7.9 Hz, 1H), 7.98 (d, J = 7.7 Hz, 2H), 7.65 (dq, J = 21.4, 7.6 Hz, 4H), 7.27 (t, J = 7.6 Hz, 1H), 2.70 (s, 3H).

4.1.3. *Tert*-butyl (3-acetylphenyl)carbamate (**1c**)

Compound **1c** was prepared in a manner similar to that described for **1a** as a white solid. Yield: 98%. ^1H NMR (400 MHz, $\text{DMSO-}d_6$) δ 9.55 (s, 1H), 8.10 (s, 1H), 7.66 (d, J = 8.0 Hz, 1H), 7.58 (d, J = 7.6 Hz, 1H), 7.41 (t, J = 7.9 Hz, 1H), 2.54 (s, 3H), 1.49 (s, 9H).

4.1.4. *N*-(3-acetylphenyl)benzamide (**1d**)

A solvent of benzoyl chloride (7.2 mmol, 1.0 g) in DCM (10 mL) was dropwise added to the mixture of 1-(2-aminophenyl)ethan-1-one (6 mmol, 0.81 g) and triethylamine (7.2 mmol, 0.72 g) in DCM (10 mL) at 0 °C and stirred for another 5 h at room temperature. Then, the mixture was poured into ice water and the pH value was adjusted to 2.0 with hydrochloric acid (2 M) and extracted with DCM. The organic layer was separated, washed with brine, dried over MgSO_4 and concentrated in vacuo. The residue was recrystallized from ethanol to give **1d** (1.2 g, 83%) as a white solid. ^1H NMR (400 MHz, $\text{DMSO-}d_6$) δ 10.46 (s, 1H), 8.39 (s, 1H), 8.09 (d, J = 8.0 Hz,

1H), 8.00 (d, J = 7.8 Hz, 2H), 7.73 (d, J = 7.6 Hz, 1H), 7.56 (td, J = 19.7, 19.2, 7.8 Hz, 4H), 2.60 (s, 3H).

4.1.5. (Z)-3-(2-(Naphthalen-1-yl)-2-oxoethylidene)-3,4-dihydroquinoxalin-2(1H)-one (**J46**)

Compound **J46** was prepared as previously reported [37]. Briefly, sodium (17.4 mmol, 400 mg) was added to a solution of ethanol (100 mL) in portions and the mixture was stirred for 1 h. The newly prepared sodium ethanol/ethanol solution was obtained. A mixture solvent of α -naphthalene ethyl ketone (10 mmol, 1.70 g) and oxalic acid diethyl ester (15 mmol, 2.19 g) was dropwise added to the aforesaid sodium ethanol/ethanol solution at 0 °C and stirred for another 4 h at room temperature. Then, the mixture was poured into ice water and the pH value was adjusted to 2.0 with hydrochloric acid (2 M). The obtained solid was filtered and washed with water (10 mL), and the crude product ethyl 4-(naphthalen-1-yl)-2,4-dioxobutanoate was used for the next step without purification. A solution of the former crude product (2.0 mmol, 540 mg) and *o*-phenylenediamine (2 mmol, 216 mg) in ethanol (10 mL) was stirred for 4 h at room temperature. The yellow solid was filtered, and the filter cake was washed with ethanol (10 mL) and water (10 mL) in sequence and then recrystallized from a mixture solvent of DMF/ethanol (15:1) to give **J46** as a yellow solid. Yield: 26%, mp 251–252 °C. ^1H NMR (400 MHz, $\text{DMSO-}d_6$) δ 13.57 (s, 1H), 12.07 (s, 1H), 8.60–8.46 (m, 1H), 8.07 (d, J = 8.2 Hz, 1H), 8.04–7.95 (m, 1H), 7.84 (d, J = 6.8 Hz, 1H), 7.67–7.52 (m, 4H), 7.25–7.09 (m, 3H), 6.58 (s, 1H). ^{13}C NMR (101 MHz, $\text{DMSO-}d_6$) δ 193.6, 156.1, 145.6, 138.7, 133.9, 131.3, 130.0, 128.9, 127.4, 127.2, 126.8, 126.7, 126.0, 125.6, 124.5, 124.5, 124.2, 117.1, 115.9, 94.2. HRMS (ESI) $[\text{M}+\text{H}]^+$ calcd for

$C_{20}H_{15}N_2O_2$: 315.1134; found: 315.1134.

4.1.6. (Z)-3-(2-(naphthalen-2-yl)-2-oxoethylidene)-3,4-dihydroquinoxalin-2(1H)-one (**J46–16**)

Compound **J46–16** was prepared in a manner similar to that described for **J46** as a yellow solid. Yield: 43%. Mp 281–282 °C. 1H NMR (400 MHz, DMSO- d_6) δ 13.74 (s, 1H), 12.09 (s, 1H), 8.65 (s, 1H), 8.18 (d, J = 7.7 Hz, 1H), 8.13–7.93 (m, 3H), 7.74–7.48 (m, 3H), 7.15 (s, 3H), 7.02 (s, 1H). ^{13}C NMR (101 MHz, DMSO- d_6) δ 188.72, 156.25, 146.03, 136.41, 134.99, 132.91, 129.95, 128.81, 128.50, 128.37, 128.03, 127.20, 124.60, 124.48, 124.17, 123.97, 117.05, 115.83, 89.91. HRMS (ESI) $[M+H]^+$ calcd for $C_{20}H_{15}N_2O_2$: 315.1134; found: 315.1142.

4.1.7. (Z)-3-(2-(2-chlorophenyl)-2-oxoethylidene)-3,4-dihydroquinoxalin-2(1H)-one (**J46–17**)

Compound **J46–17** was prepared in a manner similar to that described for **J46** as a yellow solid. Yield: 76%. Mp 252–253 °C. 1H NMR (400 MHz, DMSO- d_6) δ 13.31 (s, 1H), 12.07 (s, 1H), 7.65–7.52 (m, 3H), 7.47 (dt, J = 14.9, 6.6 Hz, 2H), 7.21–7.09 (m, 3H), 6.41 (s, 1H). ^{13}C NMR (101 MHz, DMSO- d_6) δ 190.32, 155.86, 145.57, 140.34, 131.84, 130.70, 130.23, 129.80, 127.87, 127.26, 124.73, 124.31, 124.14, 117.20, 115.87, 93.77. HRMS (ESI) $[M+H]^+$ calcd for $C_{16}H_{12}ClN_2O_2$: 299.0587; found: 299.0592.

4.1.8. (Z)-3-(2-(2-bromophenyl)-2-oxoethylidene)-3,4-dihydroquinoxalin-2(1H)-one (**J46–18**)

Compound **J46–18** was prepared in a manner similar to that described for **J46** as a yellow solid. Yield: 64%. Mp 267–268 °C. 1H NMR (400 MHz, DMSO- d_6) δ 13.24 (s, 1H), 12.09 (s, 1H), 7.71 (d, J = 8.0 Hz, 1H), 7.57 (dd, J = 15.0, 7.5 Hz, 2H), 7.49 (t, J = 7.4 Hz, 1H), 7.40 (t, J = 7.6 Hz, 1H), 7.16 (s, 3H), 6.35 (s, 1H). ^{13}C NMR (101 MHz, DMSO- d_6) δ 191.50, 155.85, 145.47, 142.47, 133.81, 131.87, 129.63, 128.36, 127.21, 124.73, 124.28, 124.16, 118.97, 117.20, 115.87, 93.57. HRMS (ESI) $[M+H]^+$ calcd for $C_{16}H_{12}BrN_2O_2$: 343.0082; found: 343.0089.

4.1.9. (Z)-3-(2-oxo-2-(*o*-tolyl)ethylidene)-3,4-dihydroquinoxalin-2(1H)-one (**J46–19**)

Compound **J46–19** was prepared in a manner similar to that described for **J46** as a yellow solid. Yield: 54%. Mp 227–228 °C. 1H NMR (400 MHz, DMSO- d_6) δ 13.40 (s, 1H), 12.01 (s, 1H), 7.59–7.52 (m, 2H), 7.42–7.36 (m, 1H), 7.30 (t, J = 7.5 Hz, 2H), 7.18–7.10 (m, 3H), 6.41 (s, 1H), 2.47 (s, 3H). ^{13}C NMR (101 MHz, DMSO- d_6) δ 193.98, 156.10, 145.28, 140.73, 136.26, 131.69, 130.52, 128.07, 127.10, 126.33, 124.52, 124.39, 124.12, 116.99, 115.83, 93.50, 20.71. HRMS (ESI) $[M+H]^+$ calcd for $C_{17}H_{15}N_2O_2$: 279.1134; found: 279.1139.

4.1.10. (Z)-3-(2-oxo-2-(2-(trifluoromethyl)phenyl)ethylidene)-3,4-dihydroquinoxalin-2(1H)-one (**J46–20**)

Compound **J46–20** was prepared in a manner similar to that described for **J46** as a yellow solid. Yield: 77%. Mp 268–269 °C. 1H NMR (400 MHz, DMSO- d_6) δ 13.17 (s, 1H), 12.11 (s, 1H), 7.84 (d, J = 7.8 Hz, 1H), 7.78 (t, J = 7.4 Hz, 1H), 7.69 (t, J = 8.0 Hz, 2H), 7.66–7.59 (m, 1H), 7.23–7.11 (m, 3H), 6.2 9 (s, 1H). ^{13}C NMR (101 MHz, DMSO- d_6) δ 191.78, 155.74, 145.66, 140.99, 133.08, 130.53, 128.90, 127.22, 127.02 (q, J = 5.3 Hz, 1C), 126.10 (q, J = 31.5 Hz, 1C), 124.81, 124.21, 124.16, 123.00, 117.26, 115.90, 93.10. ^{19}F NMR (376 MHz, DMSO- d_6) δ –56.60. HRMS (ESI) $[M+H]^+$ calcd for $C_{17}H_{12}F_3N_2O_2$: 333.0851; found: 333.0847.

4.1.11. (Z)-3-(2-(2-methoxyphenyl)-2-oxoethylidene)-3,4-dihydroquinoxalin-2(1H)-one (**J46–21**)

Compound **J46–21** was prepared in a manner similar to that described for **J46** as a yellow solid. Yield: 79%. Mp 238–239 °C. 1H NMR (400 MHz, DMSO- d_6) δ 13.56 (s, 1H), 11.95 (s, 1H), 7.68 (d,

J = 7.6 Hz, 1H), 7.48 (t, J = 7.1 Hz, 2H), 7.19–7.08 (m, 4H), 7.04 (t, J = 7.5 Hz, 1H), 6.84 (s, 1H), 3.88 (s, 3H). ^{13}C NMR (101 MHz, DMSO- d_6) δ 189.54, 157.88, 156.30, 144.91, 132.94, 130.11, 129.51, 127.14, 124.75, 124.18, 124.03, 120.94, 116.86, 115.75, 112.72, 95.42, 56.19. HRMS (ESI) $[M+H]^+$ calcd for $C_{17}H_{15}N_2O_3$: 295.1083; found: 295.1090.

4.1.12. (Z)-2-(2-(3-oxo-3,4-dihydroquinoxalin-2(1H)-ylidene)acetyl)benzonitrile (**J46–22**)

Compound **J46–22** was prepared in a manner similar to that described for **J46** as a yellow solid. Yield: 25%. Mp 376–377 °C. 1H NMR (400 MHz, DMSO- d_6) δ 12.50 (s, 1H), 11.10 (s, 1H), 8.12 (t, J = 7.4 Hz, 2H), 7.85 (d, J = 7.4 Hz, 1H), 7.77 (t, J = 7.4 Hz, 1H), 7.67 (t, J = 7.4 Hz, 1H), 7.48 (t, J = 7.6 Hz, 1H), 7.40–7.21 (m, 2H), 7.12 (s, 1H). ^{13}C NMR (101 MHz, DMSO- d_6) δ 168.71, 155.07, 154.58, 141.59, 137.82, 133.53, 132.84, 131.49, 131.34, 130.14, 128.94, 128.87, 123.93, 123.80, 121.83, 115.68, 95.70. HRMS (ESI) $[M+H]^+$ calcd for $C_{17}H_{12}N_3O_2$: 290.0930; found: 290.0938.

4.1.13. (Z)-2-(2-(3-oxo-3,4-dihydroquinoxalin-2(1H)-ylidene)acetyl)benzonitrile (**J46–24**)

Compound **J46–24** was prepared in a manner similar to that described for **J46** as a yellow solid. Yield: 13%. Mp 294–295 °C. 1H NMR (400 MHz, DMSO- d_6) δ 13.30 (s, 1H), 12.61 (s, 1H), 12.12 (s, 1H), 8.63 (d, J = 8.3 Hz, 1H), 8.06 (d, J = 7.0 Hz, 2H), 8.00 (d, J = 7.8 Hz, 1H), 7.62 (p, J = 8.1 Hz, 5H), 7.26 (t, J = 7.6 Hz, 1H), 7.17 (s, 3H), 6.84 (s, 1H). ^{13}C NMR (101 MHz, DMSO- d_6) δ 192.15, 165.26, 155.96, 146.27, 139.81, 135.00, 133.33, 132.49, 129.82, 129.46, 127.74, 127.28, 126.28, 124.90, 124.12, 123.89, 121.45, 117.72, 117.45, 115.87, 114.98, 109.99, 91.51. HRMS (ESI) $[M+H]^+$ calcd for $C_{23}H_{18}N_3O_3$: 384.1348; found: 384.1343.

4.1.14. *Tert*-butyl (Z)-2-(2-(3-oxo-3,4-dihydroquinoxalin-2(1H)-ylidene)acetyl)phenyl)carbamate (**J46–25**)

Compound **J46–25** was prepared in a manner similar to that described for **J46** as a yellow solid. Yield: 63%. Mp 243–244 °C. 1H NMR (400 MHz, DMSO- d_6) δ 13.10 (s, 1H), 12.07 (s, 1H), 10.85 (s, 1H), 8.22 (d, J = 8.4 Hz, 1H), 7.87 (d, J = 7.9 Hz, 1H), 7.58 (d, J = 6.1 Hz, 1H), 7.50 (t, J = 7.8 Hz, 1H), 7.13 (d, J = 8.9 Hz, 4H), 6.74 (s, 1H), 1.49 (s, 9H). ^{13}C NMR (101 MHz, DMSO- d_6) δ 192.10, 155.97, 152.70, 145.91, 140.06, 133.17, 129.73, 127.13, 125.24, 124.65, 124.24, 124.05, 122.36, 119.60, 117.26, 115.79, 91.47, 80.37, 28.44. HRMS (ESI) $[M+H]^+$ calcd for $C_{21}H_{22}N_3O_4$: 380.1610; found: 380.1608.

4.1.15. *Tert*-butyl (Z)-2-(2-(3-oxo-3,4-dihydroquinoxalin-2(1H)-ylidene)acetyl)phenyl)carbamate (**J46–25**)

Compound **J46–25** was prepared in a manner similar to that described for **J46** as a yellow solid. Yield: 63%. Mp 243–244 °C. 1H NMR (400 MHz, DMSO- d_6) δ 13.10 (s, 1H), 12.07 (s, 1H), 10.85 (s, 1H), 8.22 (d, J = 8.4 Hz, 1H), 7.87 (d, J = 7.9 Hz, 1H), 7.58 (d, J = 6.1 Hz, 1H), 7.50 (t, J = 7.8 Hz, 1H), 7.13 (d, J = 8.9 Hz, 4H), 6.74 (s, 1H), 1.49 (s, 9H). ^{13}C NMR (101 MHz, DMSO- d_6) δ 192.10, 155.97, 152.70, 145.91, 140.06, 133.17, 129.73, 127.13, 125.24, 124.65, 124.24, 124.05, 122.36, 119.60, 117.26, 115.79, 91.47, 80.37, 28.44. HRMS (ESI) $[M+H]^+$ calcd for $C_{21}H_{22}N_3O_4$: 380.1610; found: 380.1608.

4.1.16. (Z)-3-(2-(3-chlorophenyl)-2-oxoethylidene)-3,4-dihydroquinoxalin-2(1H)-one (**J46–26**)

Compound **J46–26** was prepared in a manner similar to that described for **J46** as a yellow solid. Yield: 26%. Mp 277–278 °C. 1H NMR (400 MHz, DMSO- d_6) δ 13.63 (s, 1H), 12.08 (s, 1H), 7.90 (d, J = 8.3 Hz, 2H), 7.61 (d, J = 7.8 Hz, 1H), 7.52 (dd, J = 15.3, 6.8 Hz, 2H), 7.13 (s, 3H), 6.75 (s, 1H). ^{13}C NMR (101 MHz, DMSO- d_6) δ 186.89, 155.94, 146.49, 140.98, 134.13, 131.95, 131.12, 127.30, 127.00, 126.08, 124.71, 124.31, 124.11, 117.17, 115.83, 89.40. HRMS (ESI) $[M+H]^+$

calcd for $C_{16}H_{12}ClN_2O_2$: 299.0587; found: 299.0597.

4.1.17. (Z)-3-(2-(3-bromophenyl)-2-oxoethylidene)-3,4-dihydroquinoxalin-2(1H)-one (**J46–27**)

Compound **J46–27** was prepared in a manner similar to that described for **J46** as a yellow solid. Yield: 55%. Mp 283–284 °C. 1H NMR (400 MHz, DMSO- d_6) δ 13.63 (s, 1H), 12.10 (s, 1H), 8.05 (s, 1H), 7.96 (d, $J = 7.8$ Hz, 1H), 7.76 (d, $J = 7.9$ Hz, 1H), 7.58–7.44 (m, 2H), 7.15 (s, 3H), 6.76 (s, 1H). ^{13}C NMR (101 MHz, DMSO- d_6) δ 186.85, 155.95, 146.51, 141.22, 134.87, 131.42, 129.93, 127.32, 126.47, 124.75, 124.34, 124.14, 122.65, 117.21, 115.85, 89.40. HRMS (ESI) $[M+H]^+$ calcd for $C_{16}H_{12}BrN_2O_2$: 343.0082; found: 343.0089.

4.1.18. (Z)-3-(2-oxo-2-(*m*-tolyl)ethylidene)-3,4-dihydroquinoxalin-2(1H)-one (**J46–28**)

Compound **J46–28** was prepared in a manner similar to that described for **J46** as a yellow solid. Yield: 64%. Mp 259–260 °C. 1H NMR (400 MHz, DMSO- d_6) δ 13.65 (s, 1H), 12.04 (s, 1H), 7.76 (d, $J = 8.7$ Hz, 2H), 7.48 (s, 1H), 7.39 (d, $J = 7.4$ Hz, 2H), 7.13 (s, 3H), 6.80 (s, 1H), 2.39 (s, 3H). ^{13}C NMR (101 MHz, DMSO- d_6) δ 189.00, 156.19, 145.92, 139.11, 138.44, 132.98, 129.06, 127.93, 127.12, 124.66, 124.57, 124.38, 124.10, 116.96, 115.80, 89.67, 21.46. HRMS (ESI) $[M+H]^+$ calcd for $C_{17}H_{15}N_2O_2$: 279.1134; found: 279.1135.

4.1.19. (Z)-3-(2-oxo-2-(3-(trifluoromethyl)phenyl)ethylidene)-3,4-dihydroquinoxalin-2(1H)-one (**J46–29**)

Compound **J46–29** was prepared in a manner similar to that described for **J46** as a yellow solid. Yield: 38%. Mp 278–279 °C. 1H NMR (400 MHz, DMSO- d_6) δ 13.71 (s, 1H), 12.14 (s, 1H), 8.28 (d, $J = 7.8$ Hz, 1H), 8.20 (s, 1H), 7.94 (d, $J = 7.7$ Hz, 1H), 7.77 (t, $J = 7.7$ Hz, 1H), 7.55 (d, $J = 6.5$ Hz, 1H), 7.16 (s, 3H), 6.83 (s, 1H). ^{13}C NMR (101 MHz, DMSO- d_6) δ 186.71, 155.91, 146.79, 139.83, 131.39, 130.54, 130.03 (q, $J = 30.0$ Hz, 1C), 128.61 (q, $J = 3.6$ Hz, 1C), 127.39, 124.85, 124.44 (d, $J = 273.4$ Hz, 1C), 124.30, 124.16, 123.62 (q, $J = 3.8$ Hz, 1C), 117.27, 115.87, 89.31. ^{19}F NMR (376 MHz, DMSO- d_6) δ –61.30. HRMS (ESI) $[M+H]^+$ calcd for $C_{17}H_{12}F_3N_2O_2$: 333.0851; found: 333.0860.

4.1.20. (Z)-3-(2-(3-methoxyphenyl)-2-oxoethylidene)-3,4-dihydroquinoxalin-2(1H)-one (**J46–30**)

Compound **J46–30** was prepared in a manner similar to that described for **J46** as a yellow solid. Yield: 48%. Mp 233–234 °C. 1H NMR (400 MHz, DMSO- d_6) δ 13.69 (s, 1H), 12.06 (s, 1H), 7.56 (d, $J = 7.6$ Hz, 1H), 7.51 (d, $J = 4.7$ Hz, 1H), 7.45 (d, $J = 7.6$ Hz, 2H), 7.14 (s, 4H), 6.79 (s, 1H), 3.83 (s, 3H). ^{13}C NMR (101 MHz, DMSO- d_6) δ 188.51, 159.96, 156.14, 146.08, 140.60, 130.34, 127.18, 124.52, 124.49, 124.14, 119.88, 118.28, 117.03, 115.82, 112.09, 89.65, 55.66. HRMS (ESI) $[M+H]^+$ calcd for $C_{17}H_{15}N_2O_3$: 295.1083; found: 295.1086.

4.1.21. (Z)-3-(2-(3-oxo-3,4-dihydroquinoxalin-2(1H)-ylidene)acetyl)benzonitrile (**J46–31**)

Compound **J46–31** was prepared in a manner similar to that described for **J46** as a yellow solid. Yield: 44%. Mp 276–277 °C. 1H NMR (400 MHz, DMSO- d_6) δ 13.69 (s, 1H), 12.11 (s, 1H), 8.33 (s, 1H), 8.26 (d, $J = 7.9$ Hz, 1H), 8.01 (d, $J = 7.6$ Hz, 1H), 7.72 (t, $J = 7.7$ Hz, 1H), 7.53 (d, $J = 7.4$ Hz, 1H), 7.15 (s, 3H), 6.82 (s, 1H). ^{13}C NMR (101 MHz, DMSO- d_6) δ 186.31, 155.87, 146.82, 139.85, 135.49, 131.93, 131.06, 130.52, 127.40, 124.90, 124.24, 124.15, 118.83, 117.32, 115.85, 112.43, 89.40. HRMS (ESI) $[M+H]^+$ calcd for $C_{17}H_{12}N_3O_2$: 290.0930; found: 290.0937.

4.1.22. (Z)-3-(2-(3-oxo-3,4-dihydroquinoxalin-2(1H)-ylidene)acetyl)benzonitrile (**J46–33**)

Compound **J46–33** was prepared in a manner similar to that described for **J46** as a yellow solid. Yield: 50%. Mp 332–333 °C. 1H NMR (400 MHz, DMSO- d_6) δ 13.68 (s, 1H), 12.06 (s, 1H), 10.46 (s, 1H),

8.48 (s, 1H), 8.08 (d, $J = 8.0$ Hz, 1H), 8.02 (d, $J = 7.3$ Hz, 2H), 7.73 (d, $J = 7.7$ Hz, 1H), 7.62 (t, $J = 7.2$ Hz, 1H), 7.54 (dt, $J = 15.6$, 7.7 Hz, 4H), 7.16 (s, 3H), 6.86 (s, 1H). ^{13}C NMR (101 MHz, DMSO- d_6) δ 188.64, 166.17, 156.21, 146.09, 140.09, 139.56, 135.23, 132.14, 129.53, 128.87, 128.16, 127.19, 124.60, 124.48, 124.14, 123.90, 122.60, 119.36, 117.06, 115.84, 89.62. HRMS (ESI) $[M+H]^+$ calcd for $C_{23}H_{18}N_3O_3$: 384.1348; found: 384.1353.

4.1.23. Tert-butyl (Z)-3-(2-(3-oxo-3,4-dihydroquinoxalin-2(1H)-ylidene)acetyl)phenyl)carbamate (**J46–34**)

Compound **J46–34** was prepared in a manner similar to that described for **J46** as a yellow solid. Yield: 42%. Mp 231–232 °C. 1H NMR (400 MHz, DMSO- d_6) δ 13.66 (s, 1H), 12.05 (s, 1H), 9.57 (s, 1H), 8.19 (s, 1H), 7.64 (d, $J = 8.0$ Hz, 1H), 7.58 (d, $J = 7.8$ Hz, 1H), 7.52 (dd, $J = 5.7$, 3.7 Hz, 1H), 7.41 (t, $J = 7.9$ Hz, 1H), 7.15 (s, 3H), 6.78 (s, 1H), 1.50 (s, 9H). ^{13}C NMR (101 MHz, DMSO- d_6) δ 188.80, 156.20, 153.27, 146.00, 140.47, 139.63, 129.52, 127.16, 124.60, 124.46, 124.15, 121.81, 121.12, 117.03, 115.83, 89.57, 79.75, 28.60. HRMS (ESI) $[M+H]^+$ calcd for $C_{21}H_{22}N_3O_4$: 380.1610; found: 380.1606.

4.1.24. (Z)-3-(2-(2,3-dichlorophenyl)-2-oxoethylidene)-3,4-dihydroquinoxalin-2(1H)-one (**J46–35**)

Compound **J46–35** was prepared in a manner similar to that described for **J46** as a yellow solid. Yield: 74%. Mp 298–299 °C. 1H NMR (400 MHz, DMSO- d_6) δ 13.24 (s, 1H), 12.13 (s, 1H), 7.74 (d, $J = 7.8$ Hz, 1H), 7.61 (d, $J = 7.2$ Hz, 1H), 7.54 (d, $J = 7.5$ Hz, 1H), 7.47 (t, $J = 7.8$ Hz, 1H), 7.16 (d, $J = 7.1$ Hz, 3H), 6.31 (s, 1H). ^{13}C NMR (101 MHz, DMSO- d_6) δ 189.59, 155.73, 145.89, 142.79, 133.03, 132.02, 129.10, 128.25, 128.03, 127.31, 124.93, 124.17, 117.34, 115.88, 93.40. HRMS (ESI) $[M+H]^+$ calcd for $C_{16}H_{11}Cl_2N_2O_2$: 333.0198; found: 333.0202.

4.1.25. (Z)-3-(2-(naphthalen-1-yl)-2-oxoethylidene)-6-nitro-3,4-dihydroquinoxalin-2(1H)-one (**J46–36**)

Compound **J46–36** was prepared in a manner similar to that described for **J46** as a yellow solid. Yield: 71%. Mp 312–313 °C. 1H NMR (400 MHz, DMSO- d_6) δ 13.16 (s, 1H), 12.36 (s, 1H), 8.71–8.42 (m, 2H), 8.16–7.76 (m, 4H), 7.57 (s, 3H), 7.18 (d, $J = 8.4$ Hz, 1H), 6.62 (s, 1H). ^{13}C NMR (101 MHz, DMSO- d_6) δ 193.63, 156.56, 144.02, 143.11, 138.12, 133.91, 132.50, 131.72, 129.94, 128.91, 127.52, 127.09, 126.72, 125.83, 125.50, 125.03, 119.32, 115.95, 112.67, 95.64. HRMS (ESI) $[M+H]^+$ calcd for $C_{20}H_{14}N_3O_4$: 360.0984; found: 360.0989.

4.1.26. (Z)-3-(2-(naphthalen-1-yl)-2-oxoethylidene)-2-oxo-1,2,3,4-tetrahydroquinoxaline-6-carbonitrile (**J46–37**)

Compound **J46–37** was prepared in a manner similar to that described for **J46** as a yellow solid. Yield: 78%. Mp 327–328 °C. 1H NMR (400 MHz, DMSO- d_6) δ 13.23 (s, 1H), 12.28 (s, 1H), 8.63–8.43 (m, 1H), 8.15 (d, $J = 1.5$ Hz, 1H), 8.09 (d, $J = 8.2$ Hz, 1H), 8.01 (dd, $J = 6.5$, 2.8 Hz, 1H), 7.86 (d, $J = 6.3$ Hz, 1H), 7.59 (qd, $J = 7.3$, 6.9, 2.8 Hz, 3H), 7.53 (dd, $J = 8.3$, 1.7 Hz, 1H), 7.21 (d, $J = 8.3$ Hz, 1H), 6.62 (s, 1H). ^{13}C NMR (101 MHz, DMSO- d_6) δ 193.79, 156.42, 144.49, 138.23, 133.93, 131.71, 130.95, 129.94, 128.95, 127.81, 127.57, 127.08, 126.77, 125.83, 125.58, 125.30, 120.74, 119.21, 116.55, 105.74, 95.32. HRMS (ESI) $[M+H]^+$ calcd for $C_{21}H_{14}N_3O_2$: 340.1086; found: 340.1085.

4.1.27. (Z)-8-methyl-3-(2-(naphthalen-1-yl)-2-oxoethylidene)-3,4-dihydroquinoxalin-2(1H)-one (**J46–38**)

Compound **J46–38** was prepared in a manner similar to that described for **J46** as a yellow solid. Yield: 66%. Mp 336–337 °C. 1H NMR (400 MHz, DMSO- d_6) δ 13.61 (s, 1H), 11.39 (s, 1H), 8.53 (d, $J = 7.8$ Hz, 1H), 8.08 (d, $J = 8.2$ Hz, 1H), 8.02 (d, $J = 7.8$ Hz, 1H), 7.87 (d, $J = 7.1$ Hz, 1H), 7.61 (t, $J = 7.2$ Hz, 3H), 7.43 (d, $J = 7.9$ Hz, 1H), 7.08 (t, $J = 7.7$ Hz, 1H), 7.02 (d, $J = 7.6$ Hz, 1H), 6.58 (s, 1H), 2.39 (s, 3H). ^{13}C

NMR (101 MHz, DMSO- d_6) δ 193.31, 156.69, 145.31, 138.60, 133.93, 131.36, 129.98, 128.91, 127.45, 126.84, 126.73, 126.25, 125.99, 125.64, 125.52, 124.71, 124.45, 123.90, 115.11, 93.76, 17.55. HRMS (ESI) $[M+H]^+$ calcd for $C_{21}H_{17}N_2O_2$: 329.1290; found 329.1298.

4.1.28. (Z)-8-bromo-3-(2-(naphthalen-1-yl)-2-oxoethylidene)-3,4-dihydroquinoxalin-2(1H)-one (**J46–39**)

Compound **J46–39** was prepared in a manner similar to that described for **J46** as a yellow solid. Yield: 20%. Mp 264–265 °C. 1H NMR (400 MHz, DMSO- d_6) δ 13.43 (s, 1H), 11.13 (s, 1H), 8.53 (d, J = 7.7 Hz, 1H), 8.10 (d, J = 8.3 Hz, 1H), 8.03 (d, J = 7.8 Hz, 1H), 7.89 (d, J = 7.1 Hz, 1H), 7.63 (dd, J = 12.3, 7.2 Hz, 4H), 7.43 (d, J = 7.9 Hz, 1H), 7.10 (t, J = 7.9 Hz, 1H), 6.62 (s, 1H). ^{13}C NMR (101 MHz, DMSO- d_6) δ 193.68, 156.69, 144.79, 138.28, 133.94, 131.63, 129.95, 128.95, 127.85, 127.56, 127.06, 126.78, 126.30, 125.90, 125.63, 125.41, 125.12, 116.75, 108.59, 94.67. HRMS (ESI) calcd $[M+H]^+$ for $C_{20}H_{14}BrN_2O_2$: 393.0239; found: 393.0249.

4.1.29. (Z)-3-(2-(2-chlorophenyl)-2-oxoethylidene)-2-oxo-1,2,3,4-tetrahydroquinoxaline-6-carbonitrile (**J46–40**)

Compound **J46–40** was prepared in a manner similar to that described for **J46** as a yellow solid. Yield: 77%. Mp 290–291 °C. 1H NMR (400 MHz, DMSO- d_6) δ 12.99 (s, 1H), 12.32 (s, 1H), 8.18 (s, 1H), 7.61 (d, J = 7.3 Hz, 1H), 7.50 (dt, J = 26.4, 6.7 Hz, 4H), 7.21 (d, J = 8.3 Hz, 1H), 6.45 (s, 1H). ^{13}C NMR (101 MHz, DMSO- d_6) δ 190.90, 156.22, 144.52, 140.06, 132.15, 131.03, 130.79, 130.25, 129.84, 128.02, 127.97, 125.15, 120.97, 119.17, 116.58, 105.71, 94.92. HRMS (ESI) $[M+H]^+$ calcd for $C_{17}H_{11}ClN_3O_2$: 324.0540; found: 324.0548.

4.1.30. (Z)-3-(2-(2-bromophenyl)-2-oxoethylidene)-2-oxo-1,2,3,4-tetrahydroquinoxaline-6-carbonitrile (**J46–41**)

Compound **J46–41** was prepared in a manner similar to that described for **J46** as a yellow solid. Yield: 72%. Mp 289–290 °C. 1H NMR (400 MHz, DMSO- d_6) δ 12.93 (s, 1H), 12.32 (s, 1H), 8.20 (s, 1H), 7.73 (d, J = 7.9 Hz, 1H), 7.62–7.47 (m, 3H), 7.42 (t, J = 7.6 Hz, 1H), 7.22 (d, J = 8.3 Hz, 1H), 6.40 (s, 1H). ^{13}C NMR (101 MHz, DMSO- d_6) δ 192.01, 156.21, 144.44, 142.20, 133.89, 132.13, 131.02, 129.66, 128.43, 128.02, 125.16, 120.97, 119.18, 118.92, 116.60, 105.71, 94.77. HRMS (ESI) $[M+H]^+$ calcd for $C_{17}H_{11}BrN_3O_2$: 368.0035; found: 368.0032.

4.1.31. (Z)-2-oxo-3-(2-oxo-2-(*o*-tolyl)ethylidene)-1,2,3,4-tetrahydroquinoxaline-6-carbonitrile (**J46–42**)

Compound **J46–42** was prepared in a manner similar to that described for **J46** as a yellow solid. Yield: 90%. Mp 291–292 °C. 1H NMR (400 MHz, DMSO- d_6) δ 13.07 (s, 1H), 12.24 (s, 1H), 8.12 (s, 1H), 7.57 (d, J = 7.3 Hz, 1H), 7.51 (d, J = 8.3 Hz, 1H), 7.40 (t, J = 7.3 Hz, 1H), 7.31 (t, J = 7.9 Hz, 2H), 7.19 (d, J = 8.3 Hz, 1H), 6.46 (s, 1H), 2.47 (s, 3H). ^{13}C NMR (101 MHz, DMSO- d_6) δ 194.37, 156.42, 144.17, 140.34, 136.48, 131.79, 130.87, 130.82, 128.20, 127.71, 126.38, 125.33, 120.67, 119.20, 116.50, 105.69, 94.70, 20.75. HRMS (ESI) $[M+H]^+$ calcd for $C_{18}H_{14}N_3O_2$: 304.1086; found: 304.1087.

4.1.32. (Z)-3-(2-(2-methoxyphenyl)-2-oxoethylidene)-2-oxo-1,2,3,4-tetrahydroquinoxaline-6-carbonitrile (**J46–43**)

Compound **J46–43** was prepared in a manner similar to that described for **J46** as a yellow solid. Yield: 10%. Mp 299–300 °C.

1H NMR (400 MHz, DMSO- d_6) δ 13.20 (s, 1H), 12.19 (s, 1H), 8.07 (s, 1H), 7.67 (s, 1H), 7.52 (s, 2H), 7.13 (d, J = 48.4 Hz, 3H), 6.87 (s, 1H), 3.89 (s, 3H). ^{13}C NMR (101 MHz, DMSO- d_6) δ 190.27, 158.02, 156.64, 143.73, 133.36, 130.94, 130.15, 129.27, 127.56, 125.58, 121.03, 120.53, 119.25, 116.44, 112.85, 105.63, 96.62, 56.26. HRMS (ESI) $[M+H]^+$ calcd for $C_{18}H_{14}N_3O_3$: 320.1035; found: 320.1042.

4.1.33. (Z)-2-oxo-3-(2-oxo-2-(*m*-tolyl)ethylidene)-1,2,3,4-tetrahydroquinoxaline-6-carbonitrile (**J46–44**)

Compound **J46–44** was prepared in a manner similar to that described for **J46** as a yellow solid. Yield: 38%. Mp 332–333 °C. 1H NMR (400 MHz, DMSO- d_6) δ 13.31 (s, 1H), 12.27 (s, 1H), 8.08 (s, 1H), 7.78 (d, J = 8.5 Hz, 2H), 7.52 (d, J = 8.2 Hz, 1H), 7.42 (d, J = 5.2 Hz, 2H), 7.19 (d, J = 8.3 Hz, 1H), 6.84 (s, 1H), 2.41 (s, 3H). ^{13}C NMR (101 MHz, DMSO- d_6) δ 189.58, 156.51, 144.89, 138.85, 138.58, 133.34, 130.92, 129.16, 128.05, 127.73, 125.39, 124.82, 120.65, 119.20, 116.50, 105.69, 90.95, 21.45. HRMS (ESI) $[M+H]^+$ calcd for $C_{18}H_{14}N_3O_2$: 304.1086; found: 304.1083.

4.1.34. (Z)-3-(2-(3-methoxyphenyl)-2-oxoethylidene)-2-oxo-1,2,3,4-tetrahydroquinoxaline-6-carbonitrile (**J46–45**)

Compound **J46–45** was prepared in a manner similar to that described for **J46** as a yellow solid. Yield: 24%. Mp 324–325 °C. 1H NMR (400 MHz, DMSO- d_6) δ 13.31 (s, 1H), 12.25 (s, 1H), 8.04 (s, 1H), 7.54 (d, J = 7.6 Hz, 1H), 7.49 (d, J = 8.3 Hz, 1H), 7.46–7.38 (m, 2H), 7.16 (t, J = 8.4 Hz, 2H), 6.79 (s, 1H), 3.83 (s, 3H). ^{13}C NMR (101 MHz, DMSO- d_6) δ 189.03, 159.96, 156.41, 145.00, 140.25, 130.92, 130.37, 127.75, 125.28, 120.64, 120.00, 119.18, 118.53, 116.49, 112.21, 105.70, 90.90, 55.67. HRMS (ESI) $[M+H]^+$ calcd for $C_{18}H_{14}N_3O_3$: 320.1035; found: 320.1041.

4.1.35. (Z)-3-(2-(2,3-dichlorophenyl)-2-oxoethylidene)-2-oxo-1,2,3,4-tetrahydroquinoxaline-6-carbonitrile (**J46–46**)

Compound **J46–46** was prepared in a manner similar to that described for **J46** as a yellow solid. Yield: 66%. Mp 327–328 °C. 1H NMR (400 MHz, DMSO- d_6) δ 12.93 (s, 1H), 12.35 (s, 1H), 8.21 (s, 1H), 7.76 (d, J = 7.8 Hz, 1H), 7.65–7.52 (m, 2H), 7.48 (t, J = 7.7 Hz, 1H), 7.21 (s, 1H), 6.36 (s, 1H). ^{13}C NMR (101 MHz, DMSO- d_6) δ 190.15, 156.07, 144.90, 142.50, 133.10, 132.26, 131.07, 129.15, 128.26, 128.16, 128.05, 125.01, 121.09, 119.14, 116.62, 105.73, 94.59. HRMS (ESI) $[M+H]^+$ calcd for $C_{17}H_{10}Cl_2N_3O_2$: 358.0150; found: 358.0150.

4.1.36. (Z)-3-(2-(2-aminophenyl)-2-oxoethylidene)-3,4-dihydroquinoxalin-2(1H)-one (**J46–23**)

A solution of compound **J46–25** (0.8 mmol, 300 mg) and tri-fluoroacetic acid (5.0 mL) in dichloromethane (5.0 mL) was stirred for 12 h at room temperature. Then, the mixture was poured into ice water and the pH value was adjusted to 8.0 with sodium bicarbonate and extracted with ethyl acetate (30 mL). The organic layer was separated, washed with brine, dried over $MgSO_4$ and concentrated in vacuo. The yellow solid was recrystallized from a mixture solvent of DMF/ethanol (15:1) to give **J46–23** as a yellow solid. Yield: 81%. Mp 375–376 °C. 1H NMR (400 MHz, DMSO- d_6) δ 13.20 (s, 1H), 11.90 (s, 1H), 7.70 (d, J = 8.0 Hz, 1H), 7.43 (d, J = 7.6 Hz, 1H), 7.21 (t, J = 7.5 Hz, 1H), 7.11 (s, 5H), 6.76 (d, J = 5.0 Hz, 2H), 6.57 (t, J = 7.4 Hz, 1H). ^{13}C NMR (101 MHz, DMSO- d_6) δ 192.73, 156.52, 151.22, 144.18, 133.53, 129.81, 126.68, 124.82, 124.07, 123.73, 119.20, 117.53, 116.39, 115.75, 115.29, 90.89. HRMS (ESI) $[M+H]^+$ calcd for $C_{16}H_{14}N_3O_2$: 280.1086; found: 280.1089.

4.1.37. (Z)-3-(2-(3-aminophenyl)-2-oxoethylidene)-3,4-dihydroquinoxalin-2(1H)-one (**J46–32**)

Compound **J46–32** was prepared in a manner similar to that described for **J46–23** as a yellow solid. Yield: 70%. Mp 259–260 °C. 1H NMR (400 MHz, DMSO- d_6) δ 13.59 (s, 1H), 11.99 (s, 1H), 7.55–7.44 (m, 1H), 7.23 (s, 1H), 7.20–7.06 (m, 5H), 6.76 (d, J = 4.9 Hz, 2H), 5.34 (s, 2H). ^{13}C NMR (101 MHz, DMSO- d_6) δ 189.79, 156.32, 149.51, 145.51, 139.92, 129.59, 127.03, 124.73, 124.21, 124.11, 117.81, 116.85, 115.79, 115.01, 112.66, 89.85. HRMS (ESI) $[M+H]^+$ calcd for $C_{16}H_{14}N_3O_2$: 280.1086; found: 280.1091.

4.2. Preparation of ligands and crystal structures

All of the chemical structures were processed using the *LigPrep* module in Schrödinger 10.2 software (Schrodinger, LLC, NY, USA) [46]. *Epik* module in Schrödinger was used to generate the ionized states and tautomers/stereoisomers at pH = 7.0 ± 2.0 [47]. The original chiralities were preserved for JNK3 inhibitors with known 3D structures, and different combinations of chiralities were generated for the decoys without 3D structures. The maximum number of stereoisomers for each decoy was set to 32 and one low-energy ring conformation was generated. The OPLS3 force field was adopted to perform energy minimization.

The crystallographic structures of the JNK3 in complex with inhibitors were retrieved from the RCSB Protein Data Bank (PDB) and crystal structure (PDB ID: 4W4W) were prepared by the *Protein Preparation Wizard* module in Schrödinger 10.2 software. Proteins were assigned bond orders, added hydrogens, protonated, removed all crystallographic water molecules and restrained minimization until the root-mean-square deviation (RMSD) lower than 0.3 Å based on the OPLS3 force field.

4.3. Molecular dynamics simulations

Following molecular docking, independent 50 ns MD simulations were performed for compound **J46–37** ligand-protein complex using the Desmond software [48]. Na⁺ and Cl[−] ions were added at physiological concentration of 0.15 M to ensure the overall neutrality of the systems. Simulations were conducted with an OPLS3 force field and a TIP3P explicit solvent model. The final size of the solvated system was close to ~50,000 atoms. We chose a 4.8 ps recording interval and the NPT ensemble was employed with a temperature fixed at 300 K and pressure at 1.01 bar. The integration time step was set at 2 fs. The model systems were relaxed using six steps default protocol implemented in Desmond, and utilized to prepare systems for production-quality simulation. Default settings were used for all other parameters. The simulation interaction diagram analysis tool was used to monitor energetics, RMSD fluctuations, hydrogen bond distances, angles, and van der Waals interactions over the simulation trajectories.

4.4. In vitro enzymatic inhibition assays

The inhibition activity against JNK3(h), JNK1α1(h), JNK2α2(h), DDR1(h), DDR2(h), EGFR(h), EGFR(L858R)(h), EGFR(L861Q)(h), EGFR(T790M)(h), EGFR(T790M,L858R)(h), were tested by Eurofins using KinaseProfiler™ Service Assay (details are available at <https://www.eurofins.com/>) [49].

JNK3(h) (JNK1α1(h) or JNK2α2(h)) was incubated with 50 mM Tris pH 7.5, 0.1 mM EGTA, 0.1% β-mercaptoethanol, 250 μM peptide (3 μM ATF2), 10 mM MgAcetate and [γ-³³P]-ATP (specific activity approx. 500 cpm/pmol, concentration as required). The reaction was initiated by the addition of the MgATP mix. After incubation for 40 min at room temperature, the reaction was terminated by the addition of 3% phosphoric acid solution. 10 μL of the reaction mixture was then spotted onto a P30 filter mat and washed three times for 5 min in 75 mM phosphoric acid and once in methanol prior to drying and scintillation counting. JNK3(h) (JNK1α1(h) or JNK2α2(h)) activity was defined as the percentage of JNK3(h) (JNK1α1(h) or JNK2α2(h)) activity in the absence of inhibitor, which was designated as 100%. IC₅₀ values were determined as the concentration in which 50% inhibition is achieved from Hill equation fitting.

DDR1(h) was incubated with 8 mM MOPS pH 7.0, 0.2 mM EDTA, 250 μM KKKSPGEYVNIEFG, 10 mM MgAcetate and [γ-³³P]-ATP (specific activity approx. 500 cpm/pmol, concentration as required).

The reaction was initiated by the addition of the MgATP mix. After incubation for 40 min at room temperature, the reaction was stopped by the addition of 3% phosphoric acid solution. 10 μL of the reaction was then spotted onto a P30 filtermat and washed three times for 5 min in 75 mM phosphoric acid and once in methanol prior to drying and scintillation counting. DDR1(h) activity was defined as the percentage of DDR1(h) activity in the absence of inhibitor, which was designated as 100%.

DDR2(h) was incubated with 8 mM MOPS pH 7.0, 0.2 mM EDTA, 250 μM KKSGRDYMTMQIG, 10 mM MnCl₂, 10 mM MgAcetate and [γ-³³P]-ATP (specific activity approx. 500 cpm/pmol, concentration as required). The reaction was initiated by the addition of the MgATP mix. After incubation for 40 min at room temperature, the reaction was stopped by the addition of 3% phosphoric acid solution. 10 μL of the reaction was then spotted onto a P30 filtermat and washed three times for 5 min in 75 mM phosphoric acid and once in methanol prior to drying and scintillation counting. DDR2(h) activity was defined as the percentage of DDR2(h) activity in the absence of inhibitor, which was designated as 100%.

EGFR (h) (EGFR(L858R)(h) or EGFR(L861Q)(h)) was incubated with 8 mM MOPS pH 7.0, 0.2 mM EDTA, 10 mM MnCl₂, 0.1 mg/mL poly(Glu, Tyr) 4:1, 10 mM MgAcetate and [γ-³³P]-ATP (specific activity approx. 500 cpm/pmol, concentration as required). The reaction was initiated by the addition of the MgATP mix. After incubation for 40 min at room temperature, the reaction was stopped by the addition of 3% phosphoric acid solution. 10 μL of the reaction was then spotted onto a Filtermat A and washed three times for 5 min in 75 mM phosphoric acid and once in methanol prior to drying and scintillation counting. EGFR(h) (EGFR(L858R)(h) or EGFR(L861Q)(h)) activity was defined as the percentage of EGFR(h) (EGFR(L858R)(h) or EGFR(L861Q)(h)) activity in the absence of inhibitor, which was designated as 100%.

EGFR(T790M)(h) or EGFR(T790M, L858R)(h) was incubated with 8 mM MOPS pH 7.0, 0.2 mM EDTA, 250 μM GGMEDIY-FFFMGGKKK, 10 mM MgAcetate and [γ-³³P]-ATP (specific activity approx. 500 cpm/pmol, concentration as required). The reaction was initiated by the addition of the MgATP mix. After incubation for 40 min at room temperature, the reaction was stopped by the addition of 3% phosphoric acid solution. 10 μL of the reaction was then spotted onto a P30 filtermat and washed three times for 5 min in 75 mM phosphoric acid and once in methanol prior to drying and scintillation counting. EGFR(T790M)(h) or EGFR(T790M, L858R)(h) activity was defined as the percentage of EGFR(T790M)(h) or EGFR(T790M, L858R)(h) activity in the absence of inhibitor, which was designated as 100%.

Declaration of competing interest

The authors declare that they have no known competing financial interests or personal relationships that could have appeared to influence the work reported in this paper.

Acknowledgements

This research was supported by the National Key Research and Development Project (Grant numbers 2019YFC1708900), the National Natural Science Foundation of China (Grant numbers 21772005), National Major Scientific and Technological Special Project for Significant New Drugs Development (2019ZX09204-001) and Beijing Natural Science Foundation (7202088, 7172118).

Appendix A. Supplementary data

Supplementary data to this article can be found online at <https://doi.org/10.1016/j.ejmech.2020.112445>.

Abbreviations

JNKs	c-Jun N-terminal kinases
MAPK	mitogen-activated protein kinase
ATP	adenosine 5'-triphosphate
ATF2	activating transcription factor 2
Elk1	ETS Transcription Factor ELK1
DPC4	deleted in pancreatic cancer locus
NFAT4	nuclear factor of activated T-Cells 4
AD	Alzheimer's disease
SAR	structure–activity relationship
IC ₅₀	half-maximal inhibitory concentration
DDR1	epithelial discoidin domain-containing receptor 1
EGFR	epidermal growth factor receptor
clogD	lipid-water partition coefficient at pH = 7.4
PDB	Protein Data Bank
HR I	hydrophobic region I
BBB	blood–brain barrier
LipE	ligand efficiency
TFA	trifluoroacetic acid
HRMS	high-resolution mass spectrometry
MD	molecular dynamics
RMSD	root mean-square deviation

References

- [1] P. Koch, M. Gehring, S.A. Laufer, Inhibitors of c-Jun N-terminal kinases: an update, *J. Med. Chem.* 58 (2015) 72–95.
- [2] C. Tournier, P. Hess, D.D. Yang, J. Xu, T.K. Turner, A. Nimnual, D. Bar-Sagi, S.N. Jones, R.A. Flavell, R.J. Davis, Requirement of JNK for stress-induced activation of the cytochrome c-mediated death pathway, *Science* 288 (2000) 870–874.
- [3] E.T. Coffey, Nuclear and cytosolic JNK signalling in neurons, *Nat. Rev. Neurosci.* 15 (2014) 285–299.
- [4] J. Cui, M. Zhang, Y.Q. Zhang, Z.H. Xu, JNK pathway: diseases and therapeutic potential, *Acta Pharmacol. Sin.* 28 (2007) 601–608.
- [5] Shane R. Bruckner, Steven P. Tammariello, Chia-Yi Kuan, Richard A. Flavell, Pasko Rakic, S. Estus, JNK3 contributes to c-Jun activation and apoptosis but not oxidative stress in nerve growth factor-deprived sympathetic neurons, *J. Neurochem.* 78 (2001) 298–303.
- [6] A. Behrens, M. Sibilio, E.F. Wagner, Amino-terminal phosphorylation of c-Jun regulates stress-induced apoptosis and cellular proliferation, *Nat. Genet.* 21 (1999) 326–329.
- [7] C. Guo, S.L. Wang, S.T. Xu, J.G. Wang, G.H. Song, SP600125 reduces lipopolysaccharide-induced apoptosis and restores the early-stage differentiation of osteoblasts inhibited by LPS through the MAPK pathway in MC3T3-E1 cells, *Int. J. Mol. Med.* 35 (2015) 1427–1434.
- [8] S. Gupta, T. Barrett, A.J. Whitmarsh, J. Cavanagh, H.K. Sluss, B. Derjard, R.J. Davis, Selective interaction of JNK protein kinase isoforms with transcription factors, *EMBO J.* 15 (1996) 2760–2770.
- [9] R.J. Davis, Signal transduction by the JNK group of MAP kinases, *Cell* 103 (2000) 239–252.
- [10] V. Waetzig, T. Herdegen, Context-specific inhibition of JNKs: overcoming the dilemma of protection and damage, *Trends Pharmacol. Sci.* 26 (2005) 455–461.
- [11] C.Y. Kuan, D.D. Yang, D.R. Samanta Roy, R.J. Davis, P. Rakic, R.A. Flavell, The Jnk1 and Jnk2 protein kinases are required for regional specific apoptosis during early brain development, *Neuron* 22 (1999) 667–676.
- [12] Kanaga Sabapathy, Yinling Hu, Tuula Kallunki, Martin Schreiber, Jean-Pierre David, Wolfram Jochum, Erwin F. Wagner, M. Karin, JNK2 is required for efficient T-cell activation and apoptosis but not for normal lymphocyte development, *Curr. Biol.* 9 (1999) 116–125.
- [13] J.T. Chen, D.H. Lu, C.P. Chia, D.Y. Ruan, K. Sabapathy, Z.C. Xiao, Impaired long-term potentiation in c-Jun N-terminal kinase 2-deficient mice, *J. Neurochem.* 93 (2005) 463–473.
- [14] R. Yarza, S. Vela, M. Solas, M.J. Ramirez, c-Jun N-terminal kinase (JNK) signaling as a therapeutic target for alzheimer's disease, *Front. Pharmacol.* 6 (2015) 321.
- [15] X. Antoniou, M. Falconi, D. Di Marino, T. Borsello, JNK3 as a therapeutic target for neurodegenerative diseases, *J. Alzheimers Dis* 24 (2011) 633–642.
- [16] J. Liu, A. Lin, Role of JNK activation in apoptosis: a double-edged sword, *Cell Res.* 15 (2005) 36–42.
- [17] G. Pirianov, K.G. Brywe, C. Mallard, A.D. Edwards, R.A. Flavell, H. Hagberg, H. Mehmet, Deletion of the c-Jun N-terminal kinase 3 gene protects neonatal mice against cerebral hypoxic-ischaemic injury, *J. Cerebr. Blood Flow Metabol.* 27 (2007) 1022–1032.
- [18] S.O. Yoon, D.J. Park, J.C. Ryu, H.G. Ozer, C. Tep, Y.J. Shin, T.H. Lim, L. Pastorino, A.J. Kunwar, J.C. Walton, A.H. Nagahara, K.P. Lu, R.J. Nelson, M.H. Tuszynski, K. Huang, JNK3 perpetuates metabolic stress induced by Abeta peptides, *Neuron* 75 (2012) 824–837.
- [19] Q. Wu, W. Wu, B. Fu, L. Shi, X. Wang, K. Kuca, JNK signaling in cancer cell survival, *Med. Res. Rev.* 39 (2019) 2082–2104.
- [20] A. Messoussi, C. Feneyrolles, A. Bros, A. Deroide, B. Daydé-Cazals, G. Chevé, N. Van Hijfte, B. Fauvel, K. Bougrin, A. Yasri, Recent progress in the design, study, and development of c-jun N-terminal kinase inhibitors as anticancer agents, *Chem. Biol.* 21 (2014) 1433–1443.
- [21] R. Schellino, M. Boido, A. Vercelli, JNK signaling pathway involvement in spinal cord neuron development and death, *Cells* (2019) 8.
- [22] A. Doma, R. Kulkarni, R. Palakodety, G.N. Sastry, J. Sridhara, A. Garlapati, Pyrazole derivatives as potent inhibitors of c-Jun N-terminal kinase: synthesis and SAR studies, *Bioorg. Med. Chem.* 22 (2014) 6209–6219.
- [23] G. Solinas, B. Becattini, JNK at the crossroad of obesity, insulin resistance, and cell stress response, *Mol Metab* 6 (2017) 174–184.
- [24] S. Papa, P.M. Choy, C. Bubici, The ERK and JNK pathways in the regulation of metabolic reprogramming, *Oncogene* 38 (2019) 2223–2240.
- [25] M. Peleli, I.K. Aggeli, A.N. Matralis, A.P. Kourounakis, I. Beis, C. Gaitanaki, Evaluation of two novel antioxidants with differential effects on curcumin-induced apoptosis in C2 skeletal myoblasts; involvement of JNKs, *Bioorg. Med. Chem.* 23 (2015) 390–400.
- [26] Y. Asano, S. Kitamura, T. Ohra, K. Aso, H. Igata, T. Tamura, T. Kawamoto, T. Tanaka, S. Sogabe, S. Matsumoto, M. Yamaguchi, H. Kimura, F. Itoh, Discovery, synthesis and biological evaluation of isoquinolones as novel and highly selective JNK inhibitors (1), *Bioorg. Med. Chem.* 16 (2008) 4715–4732.
- [27] B.L. Bennett, D.T. Sasaki, B.W. Murray, E.C. O'leary, S.T. Sakata, W. Xu, J.C. Leisten, A. Motiwala, S. Pierce, Y. Satoh, S.S. Bhagwat, A.M. Manning, D.W. Anderson, SP600125, an anthrapyrazolone inhibitor of Jun N-terminal kinase, *Proc. Natl. Acad. Sci. U. S. A.* 98 (2001) 13681–13686.
- [28] K. Kusakabe, N. Ide, Y. Daigo, Y. Tachibana, T. Itoh, T. Yamamoto, H. Hashizume, Y. Hato, K. Higashino, Y. Okano, Y. Sato, M. Inoue, M. Iguchi, T. Kanazawa, Y. Ishioka, K. Dohi, Y. Kido, S. Sakamoto, K. Yasuo, M. Maeda, M. Higaki, K. Ueda, H. Yoshizawa, Y. Baba, T. Shiota, H. Murai, Y. Nakamura, Indazole-based potent and cell-active Mps1 kinase inhibitors: rational design from pan-kinase inhibitor anthrapyrazolone (SP600125), *J. Med. Chem.* 56 (2013) 4343–4356.
- [29] M. Rahman, Z. Zhang, A.A. Mody, D.M. Su, H.K. Das, Intraperitoneal injection of JNK-specific inhibitor SP600125 inhibits the expression of presenilin-1 and Notch signaling in mouse brain without induction of apoptosis, *Brain Res.* 1448 (2012) 117–128.
- [30] H. Shen, N. Wu, Y. Wang, X. Han, Q. Zheng, X. Cai, H. Zhang, M. Zhao, JNK inhibitor SP600125 attenuates paraquat-induced acute lung injury: an in vivo and in vitro study, *Inflammation* 40 (2017) 1319–1330.
- [31] S. Halazy, Designing heterocyclic selective kinase inhibitors: from concept to new drug candidates, *ARKIVOC* (2006) 496–508.
- [32] S.S. Palmer, M. Altan, D. Denis, E.G. Tos, J.P. Gotteland, K.G. Osteen, K.L. Bruner-Tran, S.G. Nataraja, Bentamapimod (JNK inhibitor AS602801) induces regression of endometriotic lesions in animal models, *Reprod. Sci.* 23 (2016) 11–23.
- [33] V. Plantevin Krenitsky, L. Nadolny, M. Delgado, L. Ayala, S.S. Clareen, R. Hilgraf, R. Albers, S. Hegde, N. D'sidocky, J. Sapienza, J. Wright, M. Mccarrick, S. Bahmanyar, P. Chamberlain, S.L. Delker, J. Muir, D. Giegel, L. Xu, M. Celeridad, J. Lachowitz, B. Bennett, M. Moghaddam, O. Khatsenko, J. Katz, R. Fan, A. Bai, Y. Tang, M.A. Shirley, B. Benish, T. Bodine, K. Bleas, H. Raymon, B.E. Cathers, Y. Satoh, Discovery of CC-930, an orally active anti-fibrotic JNK inhibitor, *Bioorg. Med. Chem. Lett* 22 (2012) 1433–1438.
- [34] NCT01630252, JNK ClinicalTrials.gov. <https://clinicaltrials.gov/>. (Accessed 7 March 2019).
- [35] I. Khan, M.A. Tantray, M.S. Alam, H. Hamid, Natural and synthetic bioactive inhibitors of glycogen synthase kinase, *Eur. J. Med. Chem.* 125 (2017) 464–477.
- [36] K. Zheng, S. Iqbal, P. Hernandez, H. Park, P.V. Lograsso, Y. Feng, Design and synthesis of highly potent and isoform selective JNK3 inhibitors: SAR studies on aminopyrazole derivatives, *J. Med. Chem.* 57 (2014) 10013–10030.
- [37] X. Dou, H. Huang, Y. Li, L. Jiang, Y. Wang, H. Jin, N. Jiao, L. Zhang, L. Zhang, Z. Liu, Multistage screening reveals 3-substituted indolin-2-one derivatives as novel and isoform-selective c-jun N-terminal kinase 3 (JNK3) inhibitors: implications to drug discovery for potential treatment of neurodegenerative diseases, *J. Med. Chem.* 62 (2019) 6645–6664.
- [38] H. Park, S. Iqbal, P. Hernandez, R. Mora, K. Zheng, Y. Feng, P. Lograsso, Structural basis and biological consequences for JNK2/3 isoform selective aminopyrazoles, *Sci. Rep.* 5 (2015) 8047.
- [39] C.W. Murray, V. Berdini, I.M. Buck, M.E. Carr, A. Cleasby, J.E. Coyle, J.E. Curry, J.E. Day, P.J. Day, K. Hearn, A. Iqbal, L.Y. Lee, V. Martins, P.N. Mortenson, J.M. Munck, L.W. Page, S. Patel, S. Roomans, K. Smith, E. Tamanini, G. Saxty, Fragment-based discovery of potent and selective DDR1/2 inhibitors, *ACS Med. Chem. Lett.* 6 (2015) 798–803.
- [40] H. Cheng, S.K. Nair, B.W. Murray, C. Almaden, S. Bailey, S. Baxi, D. Behenna, S. Cho-Schultz, D. Dalvie, D.M. Dinh, M.P. Edwards, J.L. Feng, R.A. Ferre, K.S. Gajiwala, M.D. Hemkens, A. Jackson-Fisher, M. Jalaie, T.O. Johnson, R.S. Kania, S. Kephart, J. Lafontaine, B. Lunney, K.K. Liu, Z. Liu, J. Matthews, A. Nagata, S. Niessen, M.A. Ornelas, S.T. Orr, M. Pairish, S. Planken, S. Ren, D. Richter, K. Ryan, N. Sach, H. Shen, T. Smeal, J. Solowiej, S. Sutton, K. Tran, E. Tseng, W. Vernier, M. Walls, S. Wang, S.L. Weinrich, S. Xin, H. Xu, M.J. Yin,

- M. Zientek, R. Zhou, J.C. Kath, Discovery of 1-((3R,4R)-3-(((5-Chloro-2-((1-methyl-1H-pyrazol-4-yl)amino)-7H-pyrrolo[2,3-d]pyrimidin-4-yl)oxy)methyl)-4-methoxypyrrolidin-1-yl)prop-2-en-1-one (PF-06459988), a Potent, WT Sparing, Irreversible Inhibitor of T790M-Containing EGFR Mutants, *J. Med. Chem.* 59 (2016) 2005–2024.
- [41] M. Donnier-Marechal, P. Carato, P.E. Larchanche, S. Ravez, R. Boulahjar, A. Barczyk, B. Oxombre, P. Vermersch, P. Melnyk, Synthesis and pharmacological evaluation of benzamide derivatives as potent and selective sigma-1 protein ligands, *Eur. J. Med. Chem.* 138 (2017) 964–978.
- [42] Yu S. Andreichikov, S.G. Pitirimova, R.F. Saraeva, V.L. Gein, G.D. Plakhina, L.A. Voronova, 3-Phenacyl-2-quinolones and 3-phenacylidene-3,4-dihydro-2-quinolones, *Khimiya Geterotsiklicheskikh Soedin.* 3 (1978) 407–410.
- [43] V. Oza, S. Ashwell, L. Almeida, P. Brassil, J. Breed, C. Deng, T. Gero, M. Grondine, C. Horn, S. Ioannidis, D. Liu, P. Lyne, N. Newcombe, M. Pass, J. Read, S. Ready, S. Rowsell, M. Su, D. Toader, M. Vasbinder, D. Yu, Y. Yu, Y. Xue, S. Zabudoff, J. Janetka, Discovery of checkpoint kinase inhibitor (S)-5-(3-fluorophenyl)-N-(piperidin-3-yl)-3-ureidothiophene-2-carboxamide (AZD7762) by structure-based design and optimization of thiophenecarboxamide ureas, *J. Med. Chem.* 55 (2012) 5130–5142.
- [44] D. Shaw, S.M. Wang, A.G. Villaseñor, S. Tsing, D. Walter, M.F. Browner, J. Barnett, A. Kuglstatter, The crystal structure of JNK2 reveals conformational flexibility in the MAP kinase insert and indicates its involvement in the regulation of catalytic activity, *J. Mol. Biol.* 383 (2008) 885–893.
- [45] Y. Wang, X. Dou, L. Jiang, H. Jin, L. Zhang, L. Zhang, Z. Liu, Discovery of novel glycogen synthase kinase-3 α inhibitors: structure-based virtual screening, preliminary SAR and biological evaluation for treatment of acute myeloid leukemia, *Eur. J. Med. Chem.* 171 (2019) 221–234.
- [46] LigPrep, Version 2.3; Schrodinger, LLC, New York, 2015.
- [47] Epic, Version 3.2; Schrodinger, LLC, New York, 2015.
- [48] X. Dou, L. Jiang, Y. Wang, H. Jin, Z. Liu, L. Zhang, Discovery of new GSK-3 β inhibitors through structure-based virtual screening, *Bioorg. Med. Chem. Lett.* 28 (2018) 160–166.
- [49] R.A. Ward, P. Bethel, C. Cook, E. Davies, J.E. Debrecezi, G. Fairley, L. Feron, V. Flemington, M.A. Graham, R. Greenwood, N. Griffin, L. Hanson, P. Hopcroft, T.D. Howard, J. Hudson, M. James, C.D. Jones, C.R. Jones, S. Lamont, R. Lewis, N. Lindsay, K. Roberts, I. Simpson, S. St-Gallay, S. Swallow, J. Tang, M. Tonge, Z. Wang, B. Zhai, Structure-guided discovery of potent and selective inhibitors of ERK1/2 from a modestly active and promiscuous chemical start point, *J. Med. Chem.* 60 (2017) 3438–3450.